2017

The Actin-Severing Protein Cofilin Is Downstream Of Neuregulin Signaling, Is Regulated By The Tumor Suppressor Merlin, And Is Essential For Schwann Cell Myelination

Nicklaus Sparrow
University of Central Florida

THE ACTIN-SEVERING PROTEIN COFILIN IS DOWNSTREAM OF NEUREGULIN SIGNALING, IS REGULATED BY THE TUMOR SUPPRESSOR MERLIN, AND IS ESSENTIAL FOR SCHWANN CELL MYELINATION

by

NICKLAUS A. SPARROW
B.S. University of Central Florida, 2010

A dissertation submitted in partial fulfillment of the requirements
for the degree of Doctor of Philosophy
in the Burnett School of Biomedical Sciences
in the College of Medicine
at the University of Central Florida
Orlando, Florida

Spring Term
2017

Major Professor: Cristina Fernandez-Valle

ABSTRACT

Myelination is a complex process requiring coordination of directional motility and an increase in Schwann cell (SC) size to generate a multi-lamellar myelin sheath. Regulation of actin dynamics during myelination is poorly understood. However, it is known that myelin thickness is related to the abundance of neuregulin1-type III (NRG) expressed on the axon surface. NRG binding to ErbB2/3 receptors on the Schwann cell surface initiates signaling cascades necessary for myelination. We identify cofilin1, an actin depolymerizing and severing protein, as a downstream target of NRG-ErbB2/3 signaling in rat SC. A five minute exposure of SCs to NRG triggers phosphorylation of ErbB2 with concomitant dephosphorylation, and activation, of cofilin, and its upstream regulators, LIM domain kinase (LIMK) and Slingshot-1 phosphatase (SSH). This leads to cofilin activation and recruitment to the leading edge of the SC plasma membrane. These changes are associated with rapid plasma membrane expansion yielding a 35–50% increase in SC size within 30 minutes of NRG1 exposure. Cofilin1-deficient SCs increase phosphorylation of ErbB2, ERK, focal adhesion kinase, and paxillin in response to NRG, but fail to increase in size possibly due to stabilization of unusually long focal adhesions. Cofilin1-deficient SCs co-cultured with sensory neurons fail to elaborate myelin. Ultrastructural analysis reveals that they unsuccessfully segregate or engage axons and form only patchy basal lamina. After 48 hours of co-culturing with neurons, cofilin-deficient SCs fail to align and elongate on axons and often adhere

to the underlying substrate rather than to axons. We show that the Neurofibromatosis Type II (NF2) tumor suppressor, merlin, is an upstream regulator of cofilin1, and that merlin knockdown in Schwann cells inhibits their elaboration of normal myelin sheaths *in vitro*. Merlin-deficient SCs form shorter myelin segments in DRG neuron/SC co-cultures. Merlin-deficient Schwann cells have increased levels of both active Rac (Rac-GTP) and F-actin indicative of a stable actin cytoskeleton. Surprisingly merlin-deficient Schwann cells fail to dephosphorylate and activate cofilin1 in response to NRG stimulation. Inhibition of LIMK restores the ability of merlin-deficient SCs to activate cofilin in response to NRG. In developing rat sciatic nerve, merlin becomes hyper-phosphorylated at S518 during the time of peak myelin formation. During this time, cofilin is localized to the inner mesaxon, and subsequently to Schmidt-Lanterman incisures in mature myelin. This study: 1) identifies cofilin and its upstream regulators, LIMK and SSH, as end targets of a NRG-ErbB2/3 signaling pathway in Schwann cells, 2) demonstrates that cofilin modulates actin dynamics in Schwann cells allowing for motility needed to effectively engage and myelinate axons, 3) shows that merlin regulates NRG-ErbB2/3-cofilin-actin signaling during SC myelination to determine the myelin segment length.

For my family, above all my mother, who is and will always be my greatest support and greatest inspiration.

And for my friends, my “extended” family, who gave me perspective and, especially, encouragement when I needed it the most.

ACKNOWLEDGMENTS

I express sincere thanks and gratitude to my committee members, who have been gracious enough to facilitate this project with their wisdom and experience. Thanks go to my thesis chair, Dr. Cristina Fernandez-Valle for her unwavering belief and support in my abilities, and most importantly for her guidance throughout this endeavor.

A very special thank you goes to Marga Bott for her assistance in cell culture, and her endless and bountiful support.

TABLE OF CONTENTS

LIST OF FIGURES

LIST OF TABLES

LIST OF ABBREVIATIONS

DRGN: disassociated dorsal root ganglion neurons

LAM: laminin

LIMK: LIM domain kinase1/2

MKD-SC: merlin-deficient rat Schwann cell line; rat Schwann cells transduced with shRNAi-45

NRG: neuregulin1-type III

PAK: p21-activated kinase

PLL: poly-L-Lysine

SC(s): Schwann cell(s)

SC-94: cofilin-deficient rat Schwann cell line; rat Schwann cells transduced with shRNAi-94

SC-97: rat Schwann cell line controlling for viral transduction; rat Schwann cells transduced with shRNAi-97

SCR-SC: rat Schwann cell line rat Schwann cell line controlling for viral transduction; rat Schwann cells transduced with a random sequence shRNAi

SSH: Slingshot1 phosphatase

WT-SC: wild-type rat Schwann cells

CHAPTER ONE: GENERAL INTRODUCTION

Schwann Cells

The mammalian nervous system is divided into two physical domains: the central and peripheral nervous systems (the CNS and PNS respectively). The CNS includes the brain, brain stem, and spinal cord, while the PNS includes all nerves that extend from spinal cord and innervate tissue. The functional cell of the nervous system is the neuron, which carry the electrical signals both from the brain to target tissues (efferent signals) and from tissue back to brain (afferent signals). The essential role of neurons is supported and regulated by cells collectively known as neuroglial cells. Each one of these specialized cells performs a specific task to keep neurons healthy and functional. These cells include ependymal cells, astrocytes, oligodendrocytes, and microglia within the CNS, and satellite and Schwann cells within the PNS.

Schwann cells (SCs) are the myelinating neuroglial of the peripheral nervous system (Jessen and Mirsky 2005; Pereira et al., 2011). The multilamellar myelin sheath formed by mature SC enables the fast and efficient conduction of electric pulses (action potentials) down the axon (Fig. 1). Action potential conduction

velocity is indeed slower when the myelin sheath is absent, malformed, or damaged as it is in de-myelinating disorders such as multiple sclerosis and the various charcot-marie-tooth. SCs myelinate only one domain of a single axon; in doing so, they define the location of the node of Ranvier where action potentials are potentiated down the axon in the process of salutatory conduction. SCs originate from the neural crest and go through several developmental stages until they reach their final differentiation into either myelinating or ensheathing (non-myelinating) cells (Fig. 2). These stages include: Schwann cell precursor (SCP), immature Schwann cells (SC), and specifically for those SC that will myelinate, pro-myelinating. At birth most developing SCs are at the immature Schwann cell stage, ECM has been deposited, blood vessels have formed within the nerve, and peripheral nerves have the basic tissue structure/organization of adult nerves. At this stage, all immature SCs have the potential to become either myelinating or ensheathing SCs; this final decision is dictated by the diameter of the axon that the immature SC is in contact with. Those that are in contact with axons that have diameters larger than 1µm will myelinate, and those in contact with diameters smaller than 1 µm will ensheath. A few days after birth myelination (the process of expanding, wrapping, and compacting the adaxonal membrane) begins.

Peripheral Myelination

The myelin sheath, or simply myelin, is a multilamellar structure composed of a complex yet highly ordered mixture of lipids and proteins. Myelin-specific lipids and

proteins are only synthesized by a SC once two events occur (Simons and Trotter 2007). The first event is the establishment of a one-to-one relationship between the SC and the domain of axolemma (the axonal cell membrane of a neuron) that it will myelinate (the “pro-myelinating” stage). The second event is the deposition of extracellular matrix (ECM), specifically laminin, surrounding the SC. After these two events, the SC becomes polarized and two distinct domains of the SC plasma membrane are created: the abaxonal membrane, the outer membrane that touches the ECM, and the adaxonal membrane, the inner membrane that touches the axolemma. Genes that encode myelin proteins are turned on by transcription factors that are regulated by external signaling molecules active at each of these membranes. There are many transcription factors necessary for the production of myelin (including Sox10 and Oct6 (Jagalur et al, 2011), but Krox20 is the “master” transcription factor essential to upregulate myelin proteins, specifically protein zero (P0) and myelin basic protein (MBP) (Mirsky et al., 2008). Both of these structural proteins function to compact and hold the multiple layers of membrane within the myelin together. Although P0 is the major protein component of peripheral myelin (Giese et al., 1992), it is expressed at a lower level at early stages of development before the final differentiation of SCs, while MBP is specifically expressed by myelinating SCs and is typically used to distinguish fully differentiated SCs.

Signaling at both the abaxonal and adaxonal membranes control the development of SCs (Fig. 3). Specifically, at the abaxonal membrane, laminin within the ECM signals through integrins stimulating the activities of both FAK and the Rho family

of GTPases (RhoA, cdc42, and Rac), which in turn cause a reorganization of the actin cytoskeleton. However, at the adaxonal membrane the crucial external signaling molecule controlling the differentiation of SCs is neuregulin1-typeIII (NRG), which is expressed by neurons and anchored in the axolemma (Michailov et al., 2004; Taveggia et al., 2005). NRG activates the receptor tyrosine kinases ErbB2/ErbB3 expressed in the adaxonal membrane of the SC, initiating a multifaceted signaling cascade that causes expression and nuclear localization of Krox20. The thickness of the myelin sheath is directly proportional to the diameter of the axon and to the amount of NRG on the axolemma, and therefore, the amount of activation of the ErbB2/ErbB3 receptors. The signaling events at both the abaxonal and adaxonal membranes fine tune the expression of myelin genes and organization of the cytoskeleton in a highly-coordinated process that ultimately results in the production of the complex structure that is myelin.

Cell Migration and Cofilin

Cell migration occurs in a cycle in which the actin cytoskeleton provides not only the necessary internal cellular structure but also the force needed for the cell to migrate. In general, this cycle includes four steps: initial protrusion of the membrane in the direction of migration, attachment of the newly formed protrusion to the substratum, generation of traction force, and retraction of the tail end of the cell (Bravo-Cordero et al., 2013). During this cycle the actin cytoskeleton is dynamically reorganized undergoing repeated cycles of depolymerization and

polymerization, especially at the leading edge and tail. The tightly regulated spatial and temporal pattern of events is controlled by a plethora of actin-binding proteins involved at each step of the migration cycle. These proteins either anchor the cytoskeleton (integral membrane cell adhesion molecules along with intracellular scaffold proteins), provide the motor force to push the cell (myosin), or facilitate the depolymerization (for example gelsolin or ADF/cofilin) and polymerization (for example WASp, ARP2/3, profilin) of the cytoskeleton itself.

During the first step of the migration cycle, the ADF/cofilin protein family functions to initially depolymerize actin at the leading edge of cell allowing for an asymmetric polymerization/branching here that causes membrane protrusion (Bravo-Cordero et al., 2013). This protein family consists of ADF (actin depolymerizing factor), cofilin 1, and cofilin 2. Cofilin 1 (cofilin) is the most abundant and ubiquitous member of the family in vertebrate non-muscle tissues. Cofilin severs F-actin at the junction between cofilin-decorated and undecorated regions of F-actin by disrupting the non-covalent bonds between individual actin molecules. The severing activity of cofilin functions to one, create new sites along established F-actin strands where branching will occur (i.e., new nucleation sites), and two, replenish the pool of G-actin that will be incorporated to the new growing branches of F-actin (Fig. 4). The localized branching and expansion of cortical actin causes protrusion of the plasma membrane at the leading of edge initiating cellular migration.

Cofilin's activity is controlled in several manners including local changes in pH and binding to PIP2 in the plasma membrane. The best characterized regulation of cofilin is by phosphorylation of serine 3. Phosphorylation of serine 3 prevents cofilin from binding all forms of actin and this phosphorylation is performed by LIM-domain kinase (LIMK). The major phosphatase that actives cofilin at the leading edge is Slingshot (SSH). Both LIMK and SSH themselves are regulated by phosphorylation as well. Both enzymes are phosphorylated by p21-activated kinase (PAK) downstream of Rac. However, phosphorylation has opposite effects on these two cofilin regulating enzymes: phosphorylation of LIMK stimulates its kinase activity, while phosphorylation of SSH inhibits its phosphatase activity.

Neurofibromatosis Type II and Merlin

Neurofibromatosis Type II (NF2) is a genetic disorder that predisposes individuals to formation of multiple types of nervous system tumors (Petrilli and Fernandez-Valle 2016). These tumors include meningiomas, ependymomas, and schwannomas. The hallmark of the disease is bilateral formation of schwannomas on the eighth cranial nerve, which can cause dizziness, tinnitus, and hearing loss and ultimately deafness. Symptoms typically first appear in the late teens to early twenties with the incidence of 1 in 25,000. Although NF2 is dominantly inherited, 50–60% of cases arise from de novo mutations and can result in sporadic schwannomas.

NF2 is caused by mutations in the *Nf2* gene that encodes a tumor suppressor termed merlin, also known as schwannomin. Merlin is a member of the Band 4.1 FERM gene family (merlin is an acronym for moesin, ezrin, radixin-like protein). The proteins within this gene family link integral plasma membrane proteins to the actin cytoskeleton and exhibit a similar conformation: a N-terminal, tri-lobe cloverleaf FERM (4.1, ezrin, radixin, moesin) domain, a central –helical domain, and a c-terminal actin-binding domain (Fehon et al., 2010). The activity of ezrin, radixin, and moesin (ERM proteins) is regulated by the intramolecular interaction of the N-terminus with the C-terminus, a head-to-tail interaction. This interaction is controlled by the phosphorylation of a c-terminal threonine, which disrupts the head-to-tail interaction causing the proteins to become active and “open” allowing them to bind with plasma membrane proteins and the actin cytoskeleton. Merlin, however, is unique within the family, not only because it lacks the actin-binding domain, but it’s activity is actually inhibited by phosphorylation of the c-terminal serine 518 (Petrilli and Fernandez-Valle 2016).

Merlin regulates many signaling pathways controlling cell proliferation and survival that include receptor tyrosine kinase (RTK), cell adhesion, mammalian target of rapamycin (mTOR), PI3K/Akt and hippo pathways, and the nuclear-localized E3 ubiquitin ligase (Petrilli and Fernandez-Valle 2016). One of the earliest identified functions of merlin is its ability to inhibit the small GTPase Rac (Morrison et al., 2007) and its effector proteins the p21-activated kinases (PAK) (Kissil et al., 2003). Through this inhibition merlin indirectly regulates the actin cytoskeleton.

Gap in Knowledge

In coordination with the production of myelin proteins and new membrane, NRG signaling at the adaxonal membrane and laminin signaling at the abaxonal membrane also causes a restructuring of the SC actin cytoskeleton during myelination. This restructuring is a cyclic process of actin depolymerization followed by polymerization that creates new, branched actin filaments at the portion of the adaxonal membrane closest to the axolemma called the inner mesaxon. This process is comparable to cell migration models, and the inner measaxon is analogous with the leading edge of migrating cells. The growing actin filaments effectively push the expanding adaxonal membrane at the inner mesaxon around the axon finally giving rise to the characteristic multi-layered myelin sheath.

As in other cell types, the process of actin dynamics in SCs is governed by actin-regulating proteins that either promote the disassembly or assembly of actin filaments. Many studies have focused on the role of proteins that promote assembly of actin filaments, namely N-WASp (Jin et al., 2011; Novak et al., 2011), and profilin (Montani et al., 2014) in myelinating SCs. What is lacking in the literature are studies in myelinating SCs investigating the function, as well as upstream regulation, of actin depolymerizing proteins, such as gelsolin or ADF/cofilin.

Figures

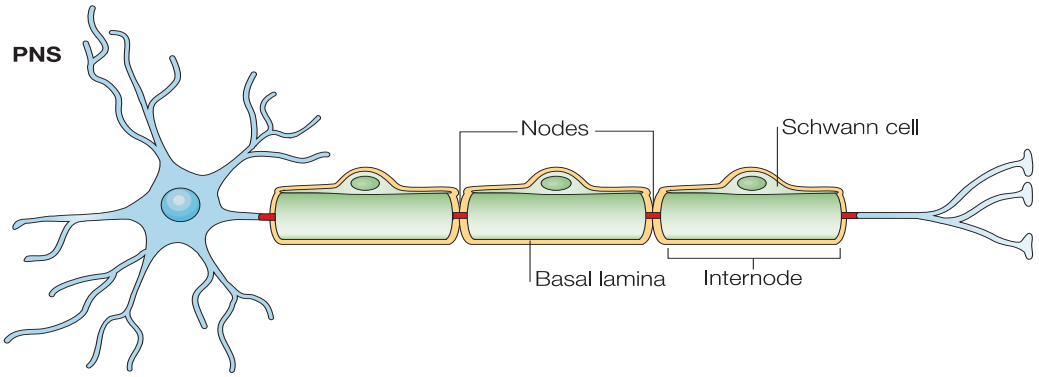

Figure 1. Illustration of a myelinated PNS axon.

“Schwann cells in the peripheral nervous system (PNS), form the myelin sheath by enwrapping their membrane several times around the axon. Myelin covers the axon at intervals (internodes), leaving bare gaps — the nodes of Ranvier.” Adapted from “The local differentiation of myelinated axons at nodes of ranvier,” by S. Poliak and E. Peles, 2003, Nature Reviews Neuroscience, 4(12), p.968-80.

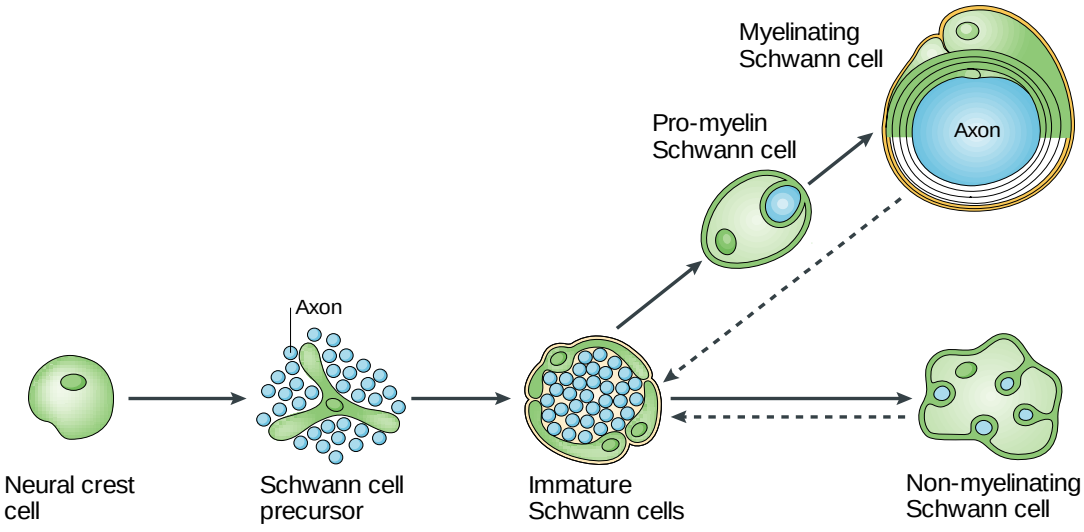

Figure 2. The development of Schwann cells.

“Schematic illustration of the main cell types and developmental transitions involved in Schwann cell development. Dashed arrows indicate the reversibility of the final, largely

postnatal transition during which mature myelinating and non- myelinating cells are generated. The embryonic phase of Schwann cell development involves three transient cell populations. First, migrating neural crest cells…second, Schwann cell precursors (SCPs)…At any one time, a rapidly developing population of cells — such as the glia of embryonic nerves — will contain some cells that are rather more advanced than others...Third, immature Schwann cells. All immature Schwann cells are considered to have the same developmental potential, and their fate is determined by the axons with which they associate. Myelination occurs only in Schwann cells that by chance envelop large diameter axons — Schwann cells that ensheath small diameter axons progress to become mature non-myelinating cells." Adapted from "The origin and development of glial cells in peripheral nerves," by K. R. Jessen and R. Mirsky, Nature Reviews Neuroscience, 6(9), p. 671-82.

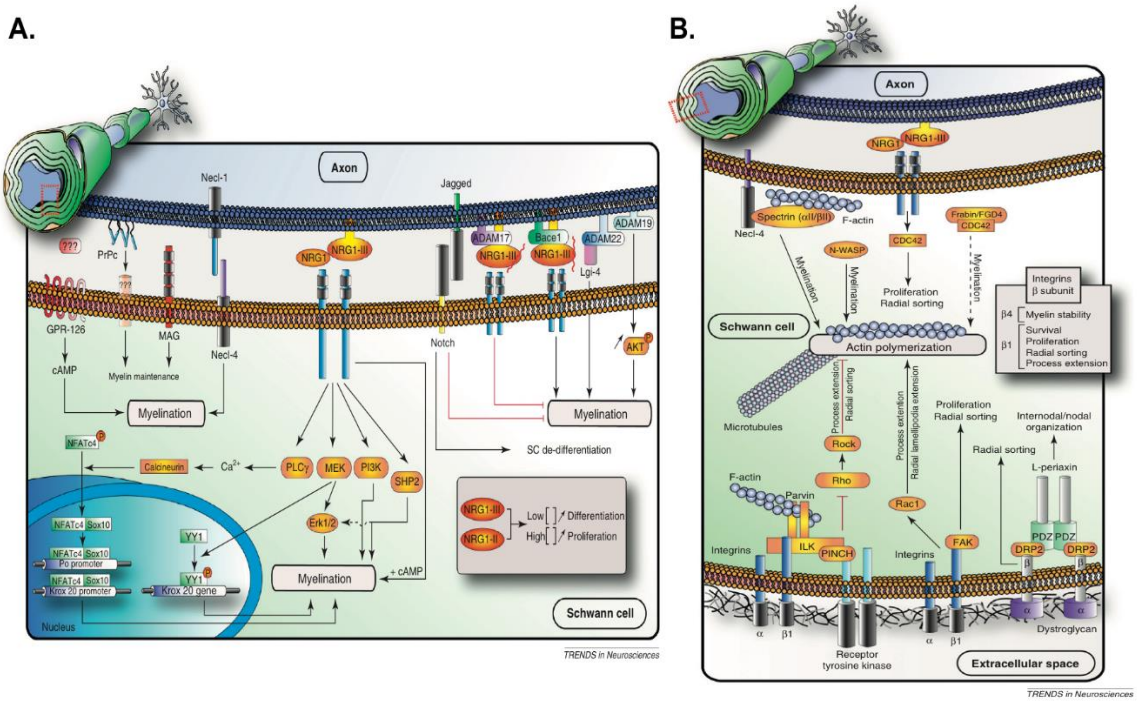

Figure 3. Molecular mechanisms controlling Schwann cell myelination.

"(A) Control of PNS myelination by SC–axon interactions. SC myelination is a process strongly dependent on instructive signals provided by the axons. Well-known mediators of this interaction, together with activated signaling pathways and their influences on myelination are shown. Arguably the most prominent axonal signal regulating myelination is NRG1, which induces a multitude of different responses through several stages of SC maturation and in myelination. Membrane-bound NRG1-III appears to play a dominant role in axon–SC signaling via a juxtacrine mechanism. (B) SC-intrinsic polarization mechanisms involved in myelination. Multiple pathways that contain SC-intrinsic polarization regulators and their crucial influence on different steps of myelination are shown. Adapted from "Molecular mechanisms regulating myelination in the peripheral nervous system," by J. A. Pereira et al., 2012, Trends in Neuroscience, 35(2), p. 123-34.

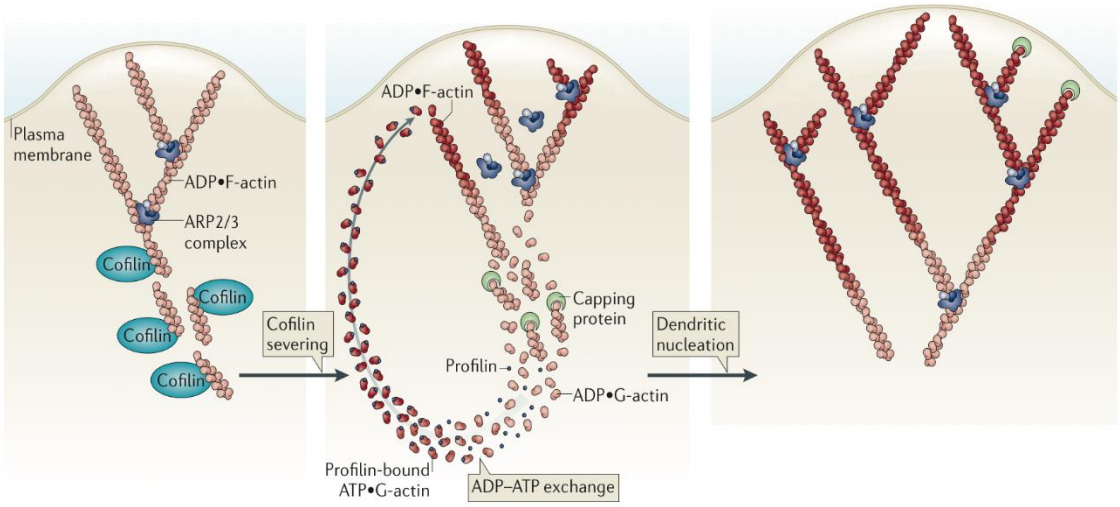

Figure 4. Diagram of cofilin function.

“Cofilin severs and depolymerizes actin filaments at the base of the lamellipodium, thereby supplying G-actin monomers for steady-state actin polymerization in conditions of G-actin depletion. Dendritic nucleation is mediated by the actin-related protein 2/3 (ARP2/3) complex. Adapted from “Functions of cofilin in cell locomotion and invasion,” by J. J. Bravo-Cordero et al., 2013, Nature Reviews Molecular Cell Biology, 14(7), p. 405-15.

CHAPTER TWO: COFILIN IS DOWNSTREAM OF NEUREGULIN SINGALING AND IS ESSENTIAL FOR SCHWANN CELL MYELINATIOIN

Introduction

Myelination is a highly specialized form of cell motility in which protrusive expansion of the leading edge of the inner mesaxon, accompanied by high rates of membrane synthesis, drives the glial membrane repeatedly around the axon to generate the myelin sheath. The hypothesis that movement of the leading edges in cell motility and myelination involve similar mechanisms is supported by experiments from the author showing a requirement for actin polymerization in myelination (Fernandez-Valle et al., 1997). This idea is supported by the essential role of Rho GTPases, molecular switches that regulate actin dynamics during cell motility, in myelination (Hall, 2005; Nodari et al., 2007).

A plethora of signaling pathways controlling actin polymerization have been identified in motile processes ranging from chemotaxis to growth cone path finding (von Philipsborn and Bastmeyer, 2007). However, the pathways linking axon contact to expansion of the Schwann cell (SC) or oligodendrocyte leading edge have not been elucidated. Key molecules directly regulating actin dynamics and organization include cofilin and actin- depolymerizing factor (ADF), also known as destrin (Oser and Condeelis, 2009). These proteins sever and depolymerize actin

filaments to generate new barbed ends to initiate actin polymerization. Although the activities of cofilin and ADF are similar and the proteins are often coexpressed in cells, they have significant functional and regulatory differences (Bernstein and Bamburg, 2010).

Cofilin1, the major form expressed in nonmuscle cells, is regulated in several ways; the best characterized is phosphorylation on serine 3 (pS3-cofilin1) that inhibits its F-actin activity (Huang et al., 2006). LIM kinases (LIMKs) 1 and 2, and the related testis kinase phosphorylate cofilin1 S3. LIMKs are serine/threonine kinases containing two LIM (Lin-11, Isl-1, and Mec3) domains and a PDZ domain. They are activated by phosphorylation on T505/508 by p21-activated kinase (PAK1 and 4) downstream of Cdc42 and Rac (Edwards et al., 1999; Dan et al., 2001), and by Rho-dependent kinase (ROCK) (Ohashi et al., 2000). Cofilin1 activity is also inhibited by binding phosphatidylinositol 4,5-bisphosphate (PIP2) at the plasma membrane (Yonezawa et al., 1990) and the scaffold protein 14-3-3 (Gohla and Bokoch, 2002). Stimulation of cofilin1 activity by dephosphorylation of serine 3 is conducted by Slingshot1 (SSH1) (Niwa et al., 2002) and chronophin phosphatases (Gohla et al., 2005). Previous studies revealed a role for pS3-cofilin1 in phospholipid signaling (Han et al., 2007; Bernstein and Bamburg, 2010). Therefore, both the phosphorylated and dephosphorylated forms of cofilin1 have potential functional activities in SCs.

A key molecule controlling myelination is neuregulin-1 (NRG1)-type III. Myelin thickness is influenced by the amount of NRG1-type III expressed on the axon's surface (Michailov et al., 2004; Taveggia et al., 2005). This membrane-anchored NRG1 isoform activates ErbB3/ ErbB2 receptors that likely regulate SC motility around the axon, in addition to SC precursor survival and proliferation (Birchmeier and Nave, 2008).

Here we report that cofilin1 is activated downstream of NRG1 signaling. Isolated cofilin1- deficient SCs activate NRG1 and laminin (LAM) signaling pathways, proliferate normally, assume a bipolar phenotype, and form focal adhesions. However, when co-cultured with sensory neurons, cofilin1-deficient SCs fail to effectively engage or align on axons, assemble a typical basal lamina, or produce myelin.

Materials And Methods

Materials And Antibodies

Mission shRNAi lentiviral transduction particles targeting mouse cofilin1, control TurboGFP and nontarget shRNAi transduction particles, and puromycin were purchased from Sigma-Aldrich. 2.5S nerve growth factor (NGF) was purchased from Harlan. AG825 (C19H15N3O3S2) was purchased from Calbiochem (manufactured by EMD) and dissolved in DMSO. Recombinant human NRG1-β1-ECD (neuregulin 1-beta 1 extracelluar domain; referred to as NRG1) was

purchased from R & D Systems and dissolved in in PBS with 0.2% BSA (fatty acid free; Sigma-Aldrich) to yield a 100 µg/ml stock solution. Reagents and antibodies for the following proteins were purchased from these sources: mouse neurofilament-H (SMI-31 and SMI-32), vinculin (hVIN-1), destrin (ADF), integrin α1, integrin β 4, collagen type IV (CTIV), and chicken neurofilament-H from Abcam; S100 from Dako; cofilin1 and pS3-cofilin1 from Novus Biologicals; pT505/508-LIMK1/2 and integrin α6 from Cell Signaling Technology; LIMK2 and laminin from Sigma-Aldrich; slingshot-1L and pS978 slingshot-1L from ECM Biosciences; Krox-20/Egr2 and myelin basic protein (MBP) from Covance; ErbB2, pY1248-ErbB2, ERK1, and pT204ERK from Santa Cruz Biotechnology; DAPI, myelin-associated glycoprotein (MAG), pY576 focal adhesion (FA) kinase (FAK), pY118 paxillin, Alexa Fluor-conjugated secondary antibodies, and Alexa Fluor 633-phalloidin from Invitrogen; paxillin, N-cadherin, FAK, and integrin β1 from BD Biosciences; and GAPDH from Millipore. All cell culture reagents were purchased from Invitrogen except for pituitary extract, purchased from Biomedical Technologies, Inc. (bti), and fetal bovine serum (FBS), purchased from Atlanta Biologicals. The LIMK inhibitor BMS-5 (C17H14Cl2F2N4OS) was purchased from Synkinase.

Preparation Of Primary Rat SCs

Primary rat (Rattus norvegicus) SCs were isolated from sciatic nerves of 1-d-old Sprague Dawley (Charles River Laboratories) pups of both sexes using the Brockes method (Brockes et al., 1979) with modifications described previously (Thaxton et al., 2011). Purified rat SCs were routinely cultured at 37°C and 5%

CO2 on 200 µg/ml poly-L-lysine (PLL)-coated (Sigma-Aldrich) dishes (Corning) in D10M [DMEM supplemented with 10% heat- inactivated FBS (HIFBS), 15 µM forskolin (Sigma-Aldrich), 20 µg/ml bovine pituitary extract, and penicillin/streptomycin (P/S; Invitrogen)].

Generation Of Cofilin1-Deficient Schwann Cell Lines

Freshly harvested and purified rat SCs were plated onto PLL-coated (200 µg/ml) six-well dishes, cultured in D10M, and maintained at 37°C and 5% CO2. When the cultures reached 70–80% confluency, lentiviral transduction particles expressing various cofilin1 shRNAi were added at various multiplicities of infection (MOIs) ranging from 0.5 to 10 in D10M plus 8 µg/ml hexadimethrine bromide (Sigma-Aldrich). After 18–20 h, the infection medium was replaced with fresh D10M for 24 h. D10M was then replaced with D10M containing 1 µg/ml puromycin (Sigma-Aldrich) for the selection of transduced cells. SCs were maintained in D10M plus puromycin and passaged (1:3 split) to expand the populations. During expansion, the cofilin1 expression level was assessed by extracting SCs directly in SDS-PAGE sample buffer and conducting Western blot analysis. ShRNAi target 94 was found to be the most efficient in reducing cofilin1 levels and was used to generate several independently derived SC lines (SC-94). SCs expressing scrambled (SCR) shRNAi did not consistently grow well. Therefore, SCs expressing shRNAi target 97 (SC-97) were used in most experiments to control for the effects of lentiviral transduction, puromycin selection, and passage number. SC-97 cells remained functional as long as cofilin1 expression dropped by no more than 30% of normal

levels and cells were passaged no more than 10 times. The presence of puromycin in the culture medium had the added benefit of eliminating fibroblasts. Independent SC lines were created on seven different occasions with different batches of lentiviral transduction particles. The degree of cofilin1 knockdown and cell function obtained with each target shRNAi was similar each time.

Preparation Of Dissociated Rat DRG Neuron/SC Co-cultures

Dorsal root ganglia (DRGs) were harvested from Sprague Dawley rat (Charles River Laboratories) embryos at 17 d of gestation [embryonic day 17 (E17)] and were dissociated as described previously (Thaxton et al., 2011). Dissociated DRG neurons (DRGNs) were plated on PLL (200 µg/ml) plus laminin (50 µg/ml; Invitrogen) or PLL plus collagen-coated (3.4 mg/ml, type I; BD Biosciences) 12 mm German glass coverslips (Carolina Biological) in CB5 medium (MEM, 0.4% glucose, 50 ng/ml 2.5S NGF and 5% HIFBS). For myelination assays, dissociated DRGN cultures were seeded with primary rat SCs or cofilin1-deficient SCs at 2 × 105 SCs per coverslip in CB10 medium (CB with 10% HIFBS). Co-cultures were then switched to myelin-permissive medium (CB with 15% HIFBS plus 0.05 mg/ml L-ascorbic acid) and were fixed 10–14 d later for ultrastructural analysis, immunostaining, or Sudan black staining.

NRG1 Stimulation And Western Blot Analysis

Normal [wild-type (WT)] SCs and cofilin1-deficient SC lines were plated on PLL-coated (200 µg/ml) six-well dishes and were grown in D10M to 50–60% confluency

(typically 72– 96 h after plating). Cultures were starved of serum and mitogens by rinsing twice in warmed HBSS (Invitrogen) and incubating in D0.5 (DMEM plus P/S plus 0.5% HIFBS). Eighteen to 22 h later, duplicate wells were stimulated for the indicated times at 37°C and 5% CO2 with D0.5 plus NRG1 carrier (PBS plus 0.02% BSA; mock medium) or D0.5 plus 10–25 ng/ml NRG1-ECD (NRG medium). For the AG825 inhibitor treatment, starved cultures were preincubated with AG825 (10 μM) in D0.5 for 1 h at 37°C and 5% CO2 and stimulated in the presence of the inhibitor. Following stimulation, wells were washed twice in PBS (Invitrogen) with phosphatase inhibitors (PIC3; Sigma-Aldrich) and were extracted directly in SDS sample buffer (Fermentas). Equal sample volumes were loaded on 4–20% precast (Pierce) or 10% self-cast polyacrylamide gels and transferred to Immobilon-P membranes (Millipore). HRP-conjugated goat secondary antibodies (Jackson ImmunoResearch) and SuperSignal West Pico Chemiluminescent Substrate (Pierce) were used for detection. Western blots were quantified using Carestream Molecular Imaging software (version 5.0). The net intensity of equivalent-sized regions of interest for phosphorylated and total proteins was obtained and normalized to GAPDH. Statistical analysis was performed from four independent experiments with GraphPad Prism 5. Stimulation experiments were analyzed using two-way ANOVA and Bonferroni's multiple comparison test. Stimulation experiments using the AG825 inhibitor were analyzed using one-way ANOVA and Tukey's multiple comparison test. We found that multiple factors influenced the consistency of the amount of phosphorylation changes. These included cell confluency, passage number, length of the starvation period, and activity of NRG1.

The activity of the NRG1 was titered before use and stored no longer than 2–3 weeks after reconstitution of the lyophilized compound. The strongest responses were observed with SC cultures at no more than 60% confluency, passaged no more than five times (1:3 splits), and starved for a minimum of 20 h. Nonstimulated WT SCs and cofilin1-deficient lines were seeded on six-well dishes coated with PLL (200 µg/ml) or PLL (200 µg/ml) plus LAM (25 µg/ml) and were grown to 60–70% confluency in D10M. Proteins were extracted in chilled TAN buffer (10 mM Tris- acetate, 1% IGEPAL, and 100 mM NaCl, with a mixture of inhibitors) following two washes in chilled PBS on ice. Three to 5 µg of total protein was loaded on 4–20% precast polyacrylamide gels (Pierce) and transferred to Immobilon-FL membranes (Millipore). Odyssey blocking buffer (LI-COR Biosciences), and secondary IRDye antibodies (LI-COR Biosciences) were used, and membranes were scanned and quantified using LI-COR Odyssey scanner and software.

Immunofluorescence Staining Of Cultures

WT-SC, SC-94, and SC-97 cultures and DRGN/SC co-cultures were immunostained as described previously (Thaxton et al., 2007). After fixation with 4% paraformaldehyde in 0.1 M phosphate buffer, myelinating co-cultures were acetone treated at −20°C with sequential exposure to 50%/100%/50% acetone for 5 min each. They were rehydrated in 0.1 M phosphate buffer and blocked for 1 h in block buffer: 0.1 M phosphate buffer plus 10% normal goat serum (Invitrogen). Myelinating co-cultures immunostained for extracellular matrix proteins were neither permeabilized nor acetone treated. Following blocking, SC- only and

nonmyelinating co-cultures were incubated with primary antibody for 1 h, while multilayered myelinating co-cultures were incubated overnight at 4°C. Secondary antibodies (goat-Alexa Fluor; Invitrogen) diluted 1:500 in block buffer were applied for 30 min. Cultures were postfixed in 4% paraformaldehyde for 5 min, stained with DAPI and, if applicable, Alexa 633-phalloidin, and were mounted in Fluorogel (Electron Microscopy Sciences). All cultures were analyzed with a Zeiss LSM710 microscope and ZEN 2009 software. Image acquisition was optimized for each antibody in triple- or quadruple-stained cultures, and fluorescence was collected on separate channels. Images were identically acquired and processed for WT-SC, SC-94, and SC-97 co-cultures, and are either single planes or maximum intensity projections as indicated in the figure legends. Focal contact/ adhesion (n = 14–32 whole cells per condition) and phalloidin mean intensity (sum pixel intensity divided by the number of pixels above background; n = 6–9 fields with 5–12 cells per field) was obtained from three independent experiments and analyzed using one-way ANOVA and Tukey's multiple comparison test with GraphPad Prism 5. Krox-20 quantification was obtained from one experiment analyzed from Z stacks (7–11 slices at a 0.5 µm interval) acquired with a 40× objective. Stacks were analyzed with Volocity 5.5 software to acquire Krox-20 cytoplasmic (sum of pixel intensities above background in a Z series minus the sum of pixel intensities colocalized with DAPI-stained nuclei) and nuclear (sum of pixel intensities colocalized with DAPI-stained nuclei) expression. Five fields were analyzed for both sets of co-cultures. Data were analyzed with GraphPad Prism 5, Student's t test.

NRG1 Stimulation-Cell Size Assay

WT SCs were seeded onto PLL-coated (200 µg/ml) 12 mm round coverslips at 5000 SCs per coverslip in D10M. Twenty-four hours later, cultures were starved for 16–18 h and then stimulated as described above for 30 min, fixed, and immunostained. For analysis, 50 individual SCs from three cultures per condition were imaged using a 20× objective. Images were analyzed using Volocity 5.5 software to measure the two-dimensional size of individual cells lacking contacts with neighboring SCs. The area was averaged for both mock- and NRG1-stimulated groups, and NRG-stimulated SC size was normalized to mock SCs. Four independent experiments were performed; p values (unpaired t test) were calculated using GraphPad Prism 5. SC-94 and SC-97 cells were seeded onto PLL- and PLL/laminin-coated 12 mm coverslips, grown for 24 h, starved for 16–18 h, and then stimulated as above for 30 min and immunostained as described above. Phalloidin-Alexa 633 fluorescence was used to calculate cell area from isolated cells (n = 16–40 cells in each condition) in three independent experiments. Statistical analysis was performed using GraphPad Prism 5, one-way ANOVA, and Tukey's multiple comparison test.

Live Imaging, Cell Attachment, And Spreading Assay

WT SCs and SC-97 and SC-94 cells were lifted by incubation in 0.05% trypsin, allowed to recover in D10M for 1 h at 37°C and 5% CO2, and seeded onto a MatTek 12-well plate coated with PLL (200 µg/ml) and laminin (25 µg/ml), with a 10 mm glass insert at 5000 cells per insert. They were immediately placed on a

Zeiss wide-field microscope with full incubation control. Three to five fields were selected for each cell type, and images were collected with a Hamamatsu ORCA camera every 3 min for 3 h using a10× phase objective and Zeiss AxioVision 4.8.2 software. Volocity 5.5 software was used to quantitate size (number of pixels) of individual cells. Four experiments were analyzed, and the mean number of pixels, SEM (n = 7 for each field), and p values (unpaired t test) were calculated using GraphPad Prism 5.

Sudan Black Staining

DRGN/SC co-cultures were prepared and analyzed as described by Chen et al. (2000). For analysis, coverslips were photographed with a 20× objective; nine of the most heavily myelinated fields were imaged on 4–16 coverslips of each WT-SC, SC-97, and SC-94 co-culture. Myelin segments in each image were manually counted and summed for each coverslip in four independent experiments. The mean, SEM, and p values (unpaired t test) were calculated using GraphPad QuickCalcs Software.

Electron Microscopy

DRGN/SC co-cultures were prepared essentially as described by Fernandez-Valle et al. (1997). The glass coverslips were removed by dissolving them in hydrofluoric acid under a fume hood. Areas of co-cultures containing neurite fascicles were selected for analysis and were either cross-sectioned or sectioned en face. Three

independent co-cultures with WT SCs and SC-94 and SC-97 cells prepared with an MOI of 5 were analyzed by electron microscopy.

Schwann Cell-Axon Alignment Assays

DRGNs cultures were seeded with WTSCs and SC-97 and SC-94 cells labeled with CellTracker Green (CTG; Invitrogen). Labeling was performed according to the manufacturer's protocol. For experiments using the LIMK inhibitor (BMS-5), labeled SCs were washed once in CB10 containing 1 μM BMS-5 before seeding in the same medium. After 24 h, the co-cultures were immunostained with neurofilament antibody and mounted as usual. For analysis, 10 randomly selected fields spanning the entire culture were imaged with a 20× objective from three cultures per condition. SC morphology was visually assessed for ~100 SCs in each type of co-culture as bipolar, tripolar, or multipolar by counting the number of processes emanating from the SC soma. The results shown for the noninhibitor study is a mean of three experiments, while the BMS-5 study is representative of two experiments. The mean, SEM, and p values (unpaired t test) were calculated using GraphPad Prism 5. For clarity, in Figure 10B, the expression of pS3-cofilin1 is shown only for SCs (pS3-cofilin1 fluorescence that colocalized with neurofilament fluorescence was subtracted after acquisition using ZEN 2009 software). pS3-Cofilin mean fluorescence intensity per cell was quantified using Volocity 5.5 software from 30 fields per condition.

Inhibitor Dose Response And Western Blot Analysis

WT SCs were seeded on PLL-coated (200 µg/ml) six-well plates and incubated at 37°C and 5% CO2 to 80–90% confluency in D10M. The medium was then replaced with fresh medium with and without serial dilutions of the LIMK inhibitor, BMS-5, and incubated for an additional 4 h. The control condition received only 0.1% of DMSO, the BMS-5 carrier. Western blot analysis was performed as described above and quantified using ImageJ software for three separate experiments. Quantitative analysis was done in Microsoft Excel software.

Results

NRG1 Promotes Dephosphorylation Of Cofilin, SSH1, And LIMK2 In SCs

To determine whether NRG1 modulates actin dynamics by regulating cofilin1 (hereafter referred to as cofilin) activity, we stimulated subconfluent starved normal SCs (WT SCs) with NRG1 for 5, 15, 30, and 60 min. WT SCs were also mock stimulated with the NRG1 carrier alone (mock). Equivalent volumes of lysate were analyzed by Western blot for phosphorylated and total levels of ErbB2 and cofilin (Fig. 1A). ErbB2 phosphorylation increased within 5 min of NRG1 stimulation and remained at three times the basal level for at least 1 h. pS3-Cofilin levels decreased by 50% within 5 min of NRG1 stimulation and remained at 30–50% of basal levels throughout the 1 h time course (Fig. 1B). To confirm that cofilin was dephosphorylated in response to ErbB2 activation, WT SCs were stimulated with NRG1 for 30 min in the presence and absence of an ErbB2 kinase inhibitor, AG825

(Osherov et al., 1993) (Fig. 1C, D). AG825 (10μM) inhibited both the phosphorylation of ErbB2 and the dephosphorylation of pS3-cofilin associated with NRG1 stimulation. NRG1 also promoted dephosphorylation of LIMK2 (T508) and SSH1 (S978) within 30 min of stimulation. Dephosphorylation of each protein was partially inhibited by AG825. The predominant isoform of LIMK detected in SCs was found to be LIMK2, and dephosphorylation of T508 reduced its kinase activity. SSH1 was expressed in SCs, and dephosphorylation of S978 activated its phosphatase activity. Thus, NRG1 promotes rapid dephosphorylation and activation of cofilin's actin depolymerizing and severing activity by regulating the activities of both LIMK2 and SSH1.

NRG1 Promotes SC Spreading And Recruitment of Cofilin To The Leading Edge

We next analyzed the cellular response of WT SCs to 30 min of NRG1 stimulation. WT SCs were immunostained with antibodies to total cofilin, ErbB2, SSH1, LIMK2, and paxillin, and F-actin was visualized with phalloidin. We observed that NRG1 induced formation of membrane protrusions and cell spreading. We used paxillin immunofluorescence to measure cell size and observed a 35 ± 6% ($p < 0.01$; $n = 4$ experiments) increase in the size of NRG1-stimulated SCs compared to mock-stimulated SCs. Cofilin was present at the leading edge of the plasma membrane and membrane protrusions in NRG1-stimulated but not in mock-stimulated SCs (Fig. 2). pS3-Cofilin antibody did not label the plasma membrane of NRG1-stimulated SCs (data not shown), suggesting that plasma membrane-associated cofilin is active. ErbB2 and SSH1 were present at the leading edge of stimulated

SCs, whereas LIMK2 was not detected at the leading edge and remained in the cytosol and processes. These results are consistent with the conclusion that NRG1 induces expansion of the SC plasma membrane by promoting cofilin recruitment, dephosphorylation, and activation at the leading edge.

Cofilin Is Essential For SC Myelination

To test the role of cofilin during myelination, we created cofilin-deficient SC lines using lentiviral delivery of cofilin shRNAi. Of the five target shRNAi tested, we found that shRNAi 94 reliably reduced cofilin protein levels by 80–90% of normal levels at an MOI of 5 (Fig. 3A–C). Cofilin shRNAi targets 95, 96, 97, and SCR promoted modest reductions in cofilin expression (10 to 30% decrease) at an MOI of 5. ShRNAi targets 94, 97, and SCR were used to generate passage-matched SC lines for analysis. Phalloidin staining and cofilin immunofluorescence revealed an increase in F-actin stress fibers and cell size in freshly plated, PLL-adherent, cofilin-deficient SC-94 cells compared to control SC-97 cells (Fig. 3D). In adhesion and spreading studies, we found that SC-94 cells adhered to laminin more quickly than SC-97 cells (compare sizes at 0.5 h) and elaborated more plasma membrane than SC-97 cells, becoming twice as large as SC-97 cells at 3.5 h of plating (Fig. 3F, G). However, when SC-94 cells reached a high cell density, they aligned with each other as bipolar cells and were morphologically indistinguishable from SC-97 (Fig. 3H) and WT SCs (data not shown). We also did not observe differences among SC-94, SC-97, and passage- matched WT SCs in proliferation rates and

cell-cycle progression as assessed with propidium iodide staining and flow cytometry (data not shown).

To assess the role of cofilin in myelination, we seeded dissociated DRGN cultures with SC-94 and SC-97 and allowed them to develop for 10–14 d in myelination-permissive medium. Sudan black stained myelin sheaths were quantified in four experiments (Fig. 4A; Table 1). We found that SC-94 cells were largely unable to produce myelin under conditions that supported myelination by SC-97 and WT SCs (data not shown). In areas of the co-culture with large axon fascicles, SC-94 cells appeared to associate with axons but did not elongate along them. An easily observable change in morphology that accompanies SC alignment and differentiation into the myelinating phenotype is nuclear elongation. This change in nuclear morphology was infrequently observed in SC-94 cells maintained for 10–14 d in myelination-permissive medium (Fig. 4A). MAG was expressed at a low level by SC-94 cells, but it was not assembled into myelin (Fig. 4B). An occasional MBP-positive SC was observed in SC-94 co-cultures; however, the immunostaining pattern of the MBP- positive segments was abnormally thin and short (Fig. 4C). The occasional myelin segments could have been synthesized by SC-94 cells expressing relatively higher cofilin levels (Fig. 3E) or residual normal SCs from the purified DRGN cultures. In contrast, SC-97 and SC- SCR cells expressed MAG and MBP that were assembled into typical myelin sheaths. We also assessed whether SC-94 cells expressed Krox-20/Egr2, a myelin-specific transcription factor. Surprisingly, the Krox-20 expression level was higher in SC-

94 than in SC-97 co-cultures; however, it largely localized to the cytosol rather than the nucleus (Fig. 4D,E). Last, the number of SCs in the co-cultures was counted to determine whether SC-94 cells failed to proliferate in contact with axons. Cell number was determined on the day after seeding onto neuron cultures as well as at the end of the 10 d myelinating period (Table 2). No differences in the number of SC-94 and SC-97 cells in the co-cultures were found. These results indicate that SC-94 cells proliferate in response to axonal NRG1 and express cytosolic Krox-20 and MAG, but fail to assemble a myelin sheath.

We conducted electron microscopic analysis of the co-cultures to assess the degree of morphological differentiation of SC-97 versus SC-94 (Fig. 5). In cross-sections, both WT SCs and SC-97 cells (Fig. 5A,B, respectively) produced compact myelin. In contrast, SC-94 cells demonstrated limited and abnormal development (Fig. 5C). Large-diameter axons often remained unsegregated (a1, a2), and many SC-94 processes failed to adhere to axons (exemplified by processes 1 and 2). A single SC-94 cell engulfed multiple relatively large- diameter axons (a3-a5) while simultaneously extending processes around other axons (processes 1, 2, and 6). This morphology indicates a failure to establish a one-to-one relationship with an axon. Additionally, this SC-94 cell produced 1.5 wraps around each of the larger-diameter axons (a3, a4) but the cytoplasmic processes were not polarized into typical mesaxons. A discontinuous basal lamina was also observed (Fig. 5C, inset, arrowheads). Whereas this amount of basal lamina deposition is not unusual for co-cultures at this stage of development, the observed

detached basal lamina is unusual. Ultrastructural analysis of *en face* sections of the co-cultures (Fig. 5D, E) confirmed the inability of SC-94 processes to form continuous close appositions with the axonal membrane. SC-97 cells formed close contacts with the axolemma (Fig. 5D, arrows); however, the processes of SC-94 cells did not adhere consistently to the axon leaving stretches of the axolemma bare (E, arrows). The ultrastructural findings suggest that cofilin-deficient SCs fail to myelinate because they are unable to effectively regulate process extension, adhere to axons, and form typical basal lamina.

Cofilin-Deficient SCs Have Abnormal Organization Of CTIV And Laminin

Because basal laminin formation and actin polymerization are needed for expression of myelin-specific genes (Fernandez-Valle et al., 1994, 1997), and detached basal lamina was observed in the ultrastructural analysis, the ability of SC-94 cells to secrete and organize basal lamina components was assessed by immunostaining. WT SCs and SC-97 and SC-94 cells were co-cultured with sensory neurons and grown for 10 d in myelination-permissive medium. Co-cultures were fixed but not permeabilized before immunostaining with antibodies to collagen type-IV (CTIV) and laminin. We found differences in the abundance and organization of CTIV and laminin in SC-94 co-cultures compared to SC-97 and WT-SC co-cultures (Fig. 6) (WT SCs not shown). CTIV was highly expressed but was organized in patches in SC-94 co-cultures, whereas it had a linear appearance in SC-97 and WT-SC co-cultures. Similarly, laminin was secreted and assembled into linear arrays in SC-97 and WT-SC co-cultures, but had an irregular distribution

in SC-94 co-cultures. These results demonstrate that cofilin- deficient SCs secrete but do not properly organize basal lamina components.

Cofilin-Deficient SCs Do Not Align On Axons

To better assess the interaction of SC-94 with axons, 10-d-old myelinating co-cultures were immunostained for the SC-specific marker S100 and for neurofilament. We observed an unusual organization of SC-94 cells in the co-cultures. Notably, cofilin-negative and S100- positive SC-94 cells adhered to the laminin substrate forming a monolayer of flat, wide bipolar cells. They did however, extend plasma membrane around neurofilament-positive neurites that contacted their surface but did not engage and align on the axons (Fig. 7). SC-97 cells expressing both cofilin and S100 adhered to axons and elongated along them as thin bipolar SCs, and minimally contacted the underlying laminin substrate. To further investigate the ability of SC-94 cells to interact with axons, we conducted axon-alignment assays using CTG-labeled SCs grown with DRGN cultures for 24 h (Fig. 8A, B). We found that SC-97 cells, expressing 90% of normal cofilin levels, assumed a bipolar morphology within 24 h of seeding onto DRGN cultures. However, SC-94 cells, expressing only 20% of normal cofilin levels, were multipolar, a morphology incompatible with axon alignment. When SC-97 lines were prepared with 10 MOI of lentiviral transduction particles (as opposed to 5 MOI), their cofilin level dropped to 60% of normal, and the frequency of multipolar SCs increased in the 24 h assay (data not shown). We also compared axon alignment of cofilin-deficient SCs after 48 h of seeding on DRGN cultures grown

on laminin versus collagen type 1 (Fig. 8C). SCs and their focal contacts and adhesions were visualized by immunostaining for vinculin. SC-94 cells failed to align along axon fascicles regardless of the substrate and the additional time. SC-97 cells aligned as bipolar cells along axons grown on both substrates. We noted that SC-94 cells formed vinculin-positive focal contacts and adhesions on the underlying substrate that could interfere with axon alignment by possibly sequestering SC processes. Alternatively, enhanced SC-94 cell adhesion to the substrate could be secondary to their inability to stabilize processes on axons. This appears more likely, as SCs are seeded on top of well-established 12-d-old neuron cultures through which SC processes must navigate before reaching the underlying substrate.

To assess whether SC-94 cells expressed normal levels of ErbB2 and integrin signaling proteins, Western blot analysis of isolated SC-94, SC-97, and WT SCs grown on laminin were conducted. The results revealed that SC-94 cells were deficient only in cofilin expression. These SCs expressed equivalent levels of the cofilin family member, ADF, as well as ErbB2, ERK1, N-cadherin, SSH1, α6 and β1 integrins, and the related signaling proteins, FAK and paxillin, which were both phosphorylated and thus active (Fig. 8D). These results suggest that SC-94 has intact ErbB2 and β1 integrin signaling pathways but is unable to modulate actin dynamics in response to receptor activity in the absence of cofilin.

Cofilin-Deficient SCs Do Not Increase In Cell Size In Response To NRG1

We analyzed the cellular and biochemical responses of SC-94, SC-97, and WT SCs grown on PLL and on laminin to 30 min of NRG1 stimulation. The cells were immunostained for vinculin to label mature focal contacts and adhesions and with phalloidin. We assessed the number and length of focal contacts/adhesions, changes in F-actin levels, and cell size (Fig. 9A,B). SC-94 cells formed fewer but longer focal contacts/adhesions than SC-97 cells on both PLL and laminin. The vinculin-positive structures present in mock-stimulated SC-94 cells had insertions of F-actin stress fibers, which define them as focal adhesions (Katoh et al., 2011). In contrast, the vinculin-positive structures formed by SC-97 cells were largely devoid of stress fibers (Fig. 9A, insets). There was no significant change in the number or length of FAs between mock- and NRG1-stimulated conditions for either cell type. NRG1 stimulation generally resulted in a reduction in the amount of F-actin compared to mock- stimulated cells that was statistically significant only in SC-97 cells grown on laminin (a 24% decrease). Whereas SC-97 cells increased in size by 50% following NRG1 stimulation on both PLL and laminin, SC-94 cells did not increase in size when grown on PLL, and decreased in size when grown on laminin (Fig. 9B). We also assessed the activity of the ErbB2 and β1 integrin signaling pathways in NRG1-stimulated WTSCs and SC-94 and SC-97 cells grown on PLL and laminin by Western blot analysis. An increase in ErbB2 phosphorylation was detected following NRG1 stimulation for all cells grown on PLL compared to the mock condition. The increase in ErbB2 phosphorylation levels was modest for all cells when grown on laminin due to a higher level of basal

activation. SC-94 cells had comparable increases in phosphorylation of ERK, FAK, and paxillin to WTSCs and SC-97 cells on both substrates (Fig. 9C). These results indicate that SC-94 cells initiate ErbB2- and β1 integrin-dependent signaling cascades in response to NRG1, but are unable to extend plasma membrane and increase in size in the absence of cofilin.

Phosphorylated Cofilin Is Necessary For SC Elongation On Axons

We examined the localization and phosphorylation states of cofilin, LIMK, and SSH1 in normal SCs cultured with axons for 24 h. To distinguish between neuronal and SC- expressed proteins, SCs were prelabeled with CellTracker Green, and axons were identified by neurofilament expression. Within 24 h of seeding onto axons, high levels of pS3-cofilin, pErbB2, pLIMK, and pSSH1 were observed in bipolar SC processes contacting axons (Fig. 10A). In unaligned, multipolar SCs, pS3-cofilin was not detected in processes and was confined to the perinuclear cytosol (Fig. 10B). To determine whether cofilin phosphorylation was needed for SCs to align on axons as bipolar cells, the experiment was repeated in the presence of BMS-5, a highly selective, potent LIMK inhibitor (Ross- Macdonald et al., 2008) (Fig. 10C). Immunostaining confirmed a decrease in phosphorylation of cofilin S3 in BMS-5 treated versus carrier-treated SCs (Fig. 10D, E). Fewer bipolar SCs were observed in 24 h co-cultures grown in the presence of BMS-5 than in control co-cultures (Fig. 10F). These results suggest that phosphorylation of cofilin S3 is needed for SCs to adopt a stable bipolar morphology in association with axons.

Discussion

The ability to rapidly expand plasma membrane is a unique biological function of myelinating SCs. Although myelin thickness has been genetically linked to the abundance of NRG1 on the axon surface (Michailov et al., 2004), the underlying pathways have not been elucidated. The present study sheds light on how NRG1 regulates actin dynamics in isolated SCs to promote expansion of the plasma membrane and an increase in cell size. Our results demonstrate that NRG1 rapidly activates cofilin's F-actin depolymerizing/severing activity in SCs and initiates membrane spreading. Moreover, we show that cofilin is required for the NRG1-induced increase in cell size. Last, we show that cofilin-deficient SCs are unable toalign or myelinate sensory axons in vitro; thus. cofilin plays an essential role during myelination.

NRG1 Stimulates A Cofilin-Dependent Increase In SC Size

Cofilin directs the site of new membrane expansion by severing and depolymerizing F-actin to generate new barbed ends for localized actin polymerization (Oser and Condeelis, 2009). Our conclusions that these activities are activated by NRG1 and required for NRG1-directed increase in SC size are supported by the results presented in Figures 1-3 and 9. We show that within 30 min of addition, NRG1 promotes a 35–50% increase in the size of WT SCs and SC-97 cells with a concomitant decrease in F-actin levels compared to the

respective mock-stimulated cells. These morphological changes are associated with NRG1/ErbB2- dependent dephosphorylation of cofilin at serine 3 that activates cofilin's actin- depolymerizing/severing activity (Figs. 1, 9). The decrease in cofilin phosphorylation arises from NRG1-stimulated dephosphorylation and inhibition of LIMK and dephosphorylation and activation of SSH1 (Fig. 1) (Oser and Condeelis, 2009). Cofilin, but not pS3-cofilin (data not shown), is concentrated at the leading edge of protrusive membranes along with ErbB2 and SSH1 phosphatase in WT SCs (Fig. 2). This suggests that recruitment to and activation of cofilin at the leading edge is responsible for initiating membrane spreading in response to NRG1. This conclusion is further supported by the failure of cofilin-deficient SC-94 cells to increase in size following NRG1 stimulation (Fig. 9), although their innate ability to adhere and spread nondirectionally on laminin is enhanced compared to SC-97 cells (Fig. 3). This is consistent with a role for cofilin in localized membrane protrusions during chemotaxis of motile cells (Ghosh et al., 2004). For example, cofilin is necessary for the response of carcinoma cells to EGF gradients (Mouneimne et al., 2006; Sidani et al., 2007). An increase in cell size and F-actin stress fibers subsequent to cofilin knockdown has been reported in other cell types (Hotulainen et al., 2005).

SC-94 cells have similar levels of expression and activation of ErbB2, N-cadherin, α6 and β1 integrins and downstream effectors, ERK1/2, FAK, and paxillin as SC-97 and WT SCs (Fig. 8). Thus, pathways needed to respond to NRG1 appear intact in cofilin-deficient SCs. The related cofilin molecule ADF is expressed in SCs, and

its expression level was unaltered following cofilin depletion. Because ADF did not functionally compensate for cofilin in SC-94 cells, it appears to have a distinct role in SCs. Overall, these studies demonstrate that cofilin is dephosphorylated in response to NRG1 stimulation and recruited to the leading edge of isolated SCs, where it participates in severing and/or depolymerizing F-actin to promote directional cell spreading.

Cofilin Is Essential For Myelination

We hypothesized that cofilin activity would be necessary for polarized expansion of the SC membrane during myelination. We sought to test this hypothesis by coculturing cofilin- deficient SCs with sensory neurons and assessing their ability to form a myelin sheath. Surprisingly, we found that cofilin-deficient SCs are unable to even effectively engage axons and stably appose them. During the initial 24–48 h of interaction, SC-94 cells fail to extend bipolar processes along axons (Fig. 8). Over the following week, SC-94 cells adhere to the laminin substrate as flattened bipolar cells and develop focal contacts/adhesions. Isolated SC-94 cells form atypically long focal adhesions on both PLL and laminin compared to the focal contacts/adhesions formed by SC-97 cells (Fig. 9). It has been shown that focal adhesion turnover requires cofilin and F-actin depolymerization (Gupton et al., 2007; Marshall et al., 2009; Maruthamuthu et al., 2010). The aberrant adhesion and spreading of SC-94 cells on the substrate could be a consequence of their inability to stably engage axons in the absence of cofilin and is discussed below.

While our standard myelination assay is conducted over 10–14 d, SC-94/DRGN co-cultures grown for 4 weeks in myelin-permissive medium did not further differentiate (data not shown), indicating that SC-94 cells were not simply delayed in differentiation. We also did not find differences in the number of DAPI- and Ki67-positive SC-94 cells in the DRGN cultures compared to controls (Table 2) (data not shown), indicating that cofilin-deficient SCs proliferate in response to axonal NRG1. Our analysis of the ErbB2 and β1 integrin pathways in isolated SC-94 cells and their ability to proliferate in response to soluble and axonal-NRG1 suggest that cofilin-deficient SCs activate pathways necessary for differentiation but cannot execute directed morphological changes in the absence of cofilin. This is supported by the low-level expression of MAG and cytosolic Krox-20 in SC-94 compared with controls. Translocation of Krox-20 into the nucleus is regulated by its interaction with 14-3-3 protein that maintains it in the cytoplasm (Dillon et al., 2007). Because cofilin directly binds 14-3-3 (Gohla and Bokoch 2002), loss of expression of this abundant protein in SCs could increase levels of free 14-3-3, thereby perturbing the balance of nuclear/cytosolic Krox-20 and contributing to the inability of SC-94 cells to myelinate. Contact between the SC and axon is needed for development of basal lamina. The deposition of basal lamina by cofilin-deficient SCs resembled that reported in studies in which direct contact between SCs and axons was prevented (Clark and Bunge, 1989). This early study revealed that SCs assemble normal-appearing basal lamina only when they ensheathe axons. Thus, the abnormal distribution of laminin and basal lamina in SC-94/DRGN co-cultures could arise from their inability to stably engage axons as elongated bipolar cells.

Abnormal laminin deposition and consequent aberrant motility have also been reported in keratinocytes and arose from deregulation of β4 integrin signaling to Rac1 and cofilin1 (Sehgal et al., 2006).

Phosphorylated Cofilin Plays A Role In SC Engagement Of Axons

SC-94 cells retain the ability to extend plasma membrane around axons but do so in an “unregulated” manner, as shown in Figure 5 and 7. Cofilin-deficient SCs engulf and wrap multiple axons at once, intermittently contact others, and fail to segregate larger-diameter axons. The inability to closely appose and adhere to axons could be due to an inability to stabilize their cytoskeleton in response to ErbB2 activation in the absence of cofilin. This possibility is supported by the distribution of pS3-cofilin in normal SC/DRGN co-cultures (Fig. 10). Bipolar SC processes contained higher levels of phosphorylated cofilin S3, LIMK, and SSH1 than multipolar processes of axon-associated SCs. Moreover, inhibition of LIMK activity reduced pS3-cofilin levels in SCs, and concomitantly their ability to align bipolar processes on axons. This suggests that cofilin S3 phosphorylation plays a role during early differentiation and is needed to stabilize SC–axon contacts during axon engagement. Previously, phosphorylated ErbB2 and the Cdc42/Rac guanine exchange factor Dock7 were shown to be present at the leading edge of membrane protrusions in migrating SCs (Yamauchi et al., 2008). Thus, NRG1 could stimulate Cdc42/Rac-PAK1-dependent phosphorylation and activation of LIMK, leading to cofilin S3 phosphorylation during the initial alignment of SC on axons. Alternatively, cofilin could be phosphorylated in response to β1 integrin

activation of Cdc42/Rac/Pak or Rho/ROCK, both of which phosphorylate LIMK. ROCK has been shown to play a role in SC myelination (Melendez-Vasquez et al., 2004).

Previous studies suggested that pS3-cofilin plays an important role in phospholipid signaling (Bernstein and Bamburg, 2010) by binding and sequestering PIP2 on the membrane (van Rheenen et al., 2007). A role for PIP3 in myelination has been demonstrated previously (Goebbels et al., 2010). A concomitant decrease in PIP2 levels observed in PTEN (phosphate and tensin homolog)-null sciatic nerves could lead to rampant cofilin activation and contribute to the observed hypermyelination. Additionally, pS3-cofilin directly stimulates phospholipase D1 in response to receptor activation (Han et al., 2007). This enzyme is regulated by Rho GTPases, protein kinase C, and PIP2 (Rudge and Wakelam, 2009). Phosphatidic acid regulates integrin-dependent adhesion and cytoskeletal remodeling, binds mTOR (mammalian target of rapamycin) and S6 kinase, and enriches the Rac guanine exchange factor DOCK2 at the leading edge of neutrophils (Gomez-Cambronero, 2010). Hence, the phenotype observed in cofilin-deficient SCs potentially reflects deregulation of phospholipid signaling as well as actin dynamics.

Cofilin is an end target for both NRG1 and laminin signaling. Our results support the conclusion that the spatiotemporal balance of phosphorylated and dephosphorylated cofilin S3 regulates SC function during myelination. During axon engagement, an increase in cofilin S3 phosphorylation would stabilize F-actin and

decrease process motility, allowing adhesive SC–axon interactions to develop. During active myelination, dephosphorylation of cofilin S3 triggers directed expansion of the plasma membrane in response to NRG1. A working model summarizing our results is presented in Figure 11. Future studies will test the hypothesis that localized cofilin dephosphorylation along the inner mesaxon contributes to its motility during active myelination.

Figures And Tables

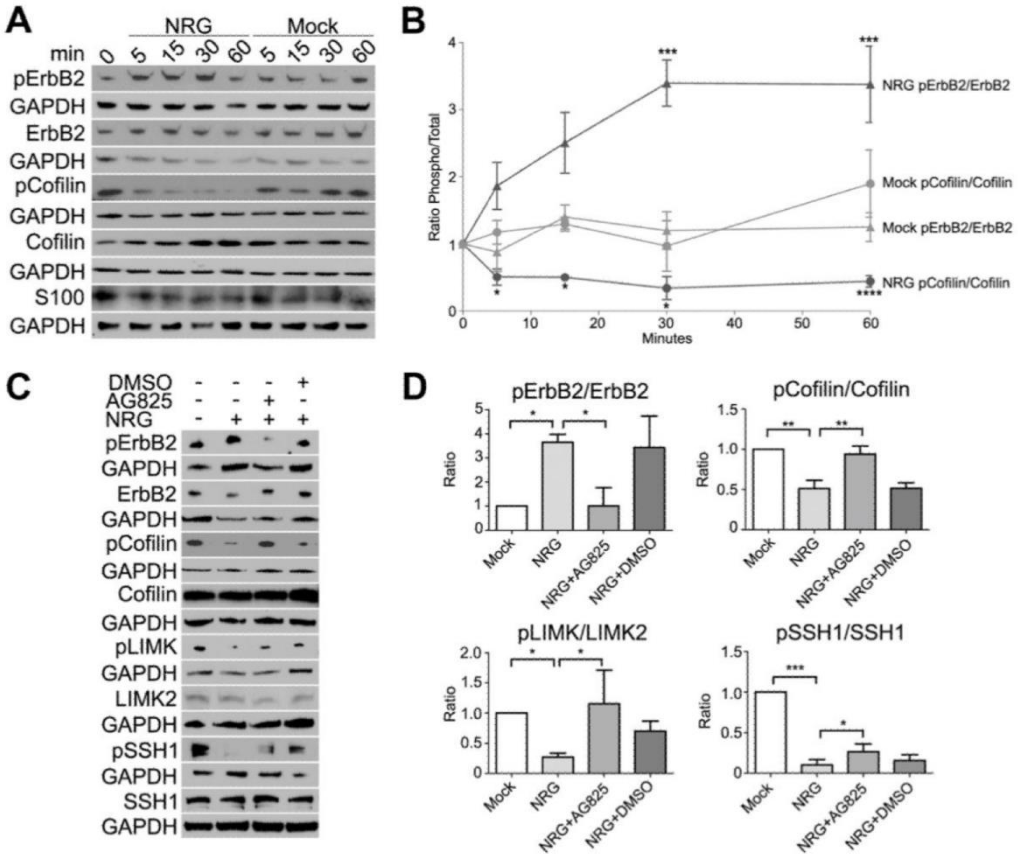

Figure 5. NRG1 promotes dephosphorylation of cofilin, LIMK2, and SSH1 in SCs.

(A) Subconfluent normal (WT-SC) cultures grown on PLL-coated wells were starved of serum and mitogens overnight by incubation in DMEM containing 0.5% FBS (D0.5). They were stimulated with D0.5 plus NRG1 (NRG) or with fresh D0.5 plus NRG1 carrier (Mock)

for the indicated times and were extracted in SDS sample buffer. Equal volumes were used in Western blot analysis with the indicated antibodies recognizing total and phosphorylated epitopes (pS3- cofilin and pY1248-ErbB2) and GAPDH. S100 was used as an SC marker. (B) Quantification of the global changes in phosphorylation following NRG1 stimulation is shown. The graph depicts the mean and SEM of the ratio of normalized phosphorylated/total protein in four independent experiments for each time point. (C) Subconfluent WT SCs grown on PLL were starved and stimulated as above for 30 min in the presence and absence of (20μM) AG825, an ErbB2 inhibitor. Western blots were performed with total and phospho-antibodies (pS978-SSH1 and pT505/508-LIMK1/2). (D) The mean and SEM of the normalized ratio of phosphorylated to total protein after normalization of each to the Mock condition is shown for four independent experiments. NRG1 promotes ErbB2 phosphorylation and cofilin dephosphorylation with similar time courses. AG825 inhibits ErbB2 phosphorylation and decreases dephosphorylation of cofilin, LIMK, and SSH1. *p < 0.05; **p < 0.01; ***p < 0.001; ****p < 0.0001.

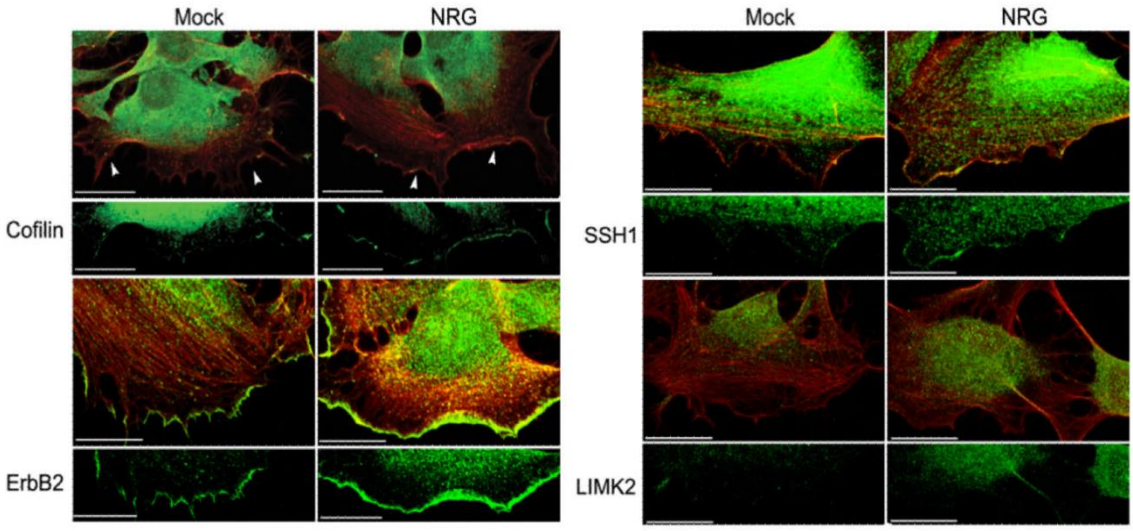

Figure 6. Cofilin is recruited to the leading edge in response to NRG1.

Subconfluent SC cultures grown on PLL-coated glass coverslips were starved and stimulated as described in Figure 1 for 30 min. They were immunostained with antibodies to total cofilin, ErbB2, SSH1, and LIMK2 (all shown in green) and with phalloidin (red). In mock-stimulated cells, only ErbB2 was present at the plasma membrane. In NRG1-stimulated cells, cofilin, ErbB2, and SSH1 were present in the cytosol as well as at the leading edge of plasma membrane protrusions. LIMK2 was localized predominantly in the cytosol and in processes in NRG-stimulated cells, and was not observed at the leading edge. All images are maximum intensity projections of six-slice Z stacks using a 0.5 μ minterval. Arrowheads indicate the leading edge of the plasma membrane. Scale bars: 20 μm.

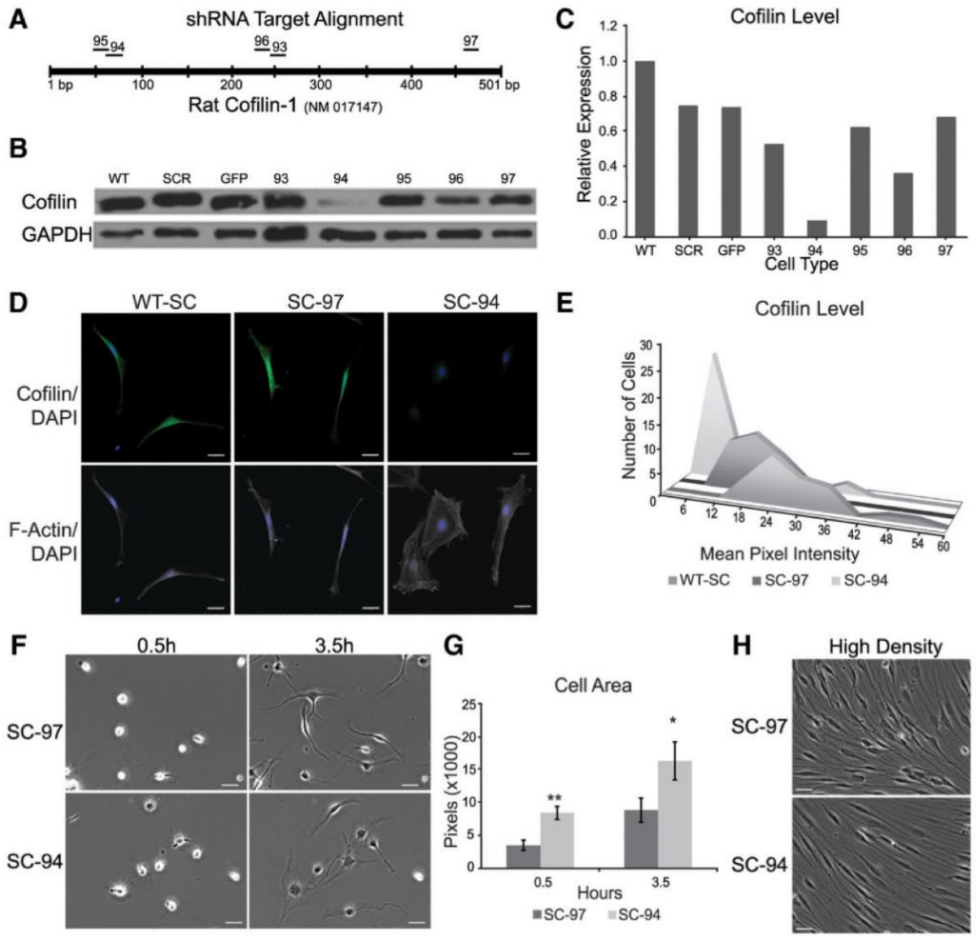

Figure 7. Generation of cofilin-deficient Schwann cells. Lentiviral delivery of cofilin shRNAi was used to create cofilin-deficient SCs.

(A) Schematic alignment of the shRNAi targets 93–97 on rat (Rattus norvegicus) cofilin-1 (NM017147) is shown. B, Western blots reveal the protein levels of cofilin and GAPDH in stable lentiviral-transduced (5 MOI) WTSCs expressing SCR and TurboGFP and shRNAi targets 93–97. (C) Quantification of cofilin levels (B) normalized to GAPDH and expressed relative to WTSCs. (D) Immunofluorescence staining for cofilin and F-actin using phalloidin in WTSCs and stable SC-97 and SC-94 lines verifies that SC-94 cells express low levels of cofilin, while WT SCs and SC-97 cells express cofilin. Phalloidin staining shows an increase in F-actin stress fibers and cell size in SC-94 compared to controls. (E) Quantification of cofilin levels (D) of 20–30 individual WTSCs and SC-97 and SC-94 cells show a distribution of cofilin expression levels. (F) SC-94 and SC-97 cells were seeded onto laminin-coated glass coverslips and imaged in real time for 3.0 h beginning 0.5 h after seeding in five separate experiments. Frames captured at 0.5 and 3.5 h are shown and reveal that SC-94 cells attach to laminin more quickly and spread more plasma membrane than control SC-97 cells. (G) Quantification of cell size is shown in F. *$p < 0.05$; **$p < 0.002$. (H) Images of SC-94 and SC-97 grown on PLL-coated glass coverslips reveal that cofilin deficiency in SC-94 cells does not interfere with acquisition of a bipolar morphology at high cell density. Scale bars: 20 μm.

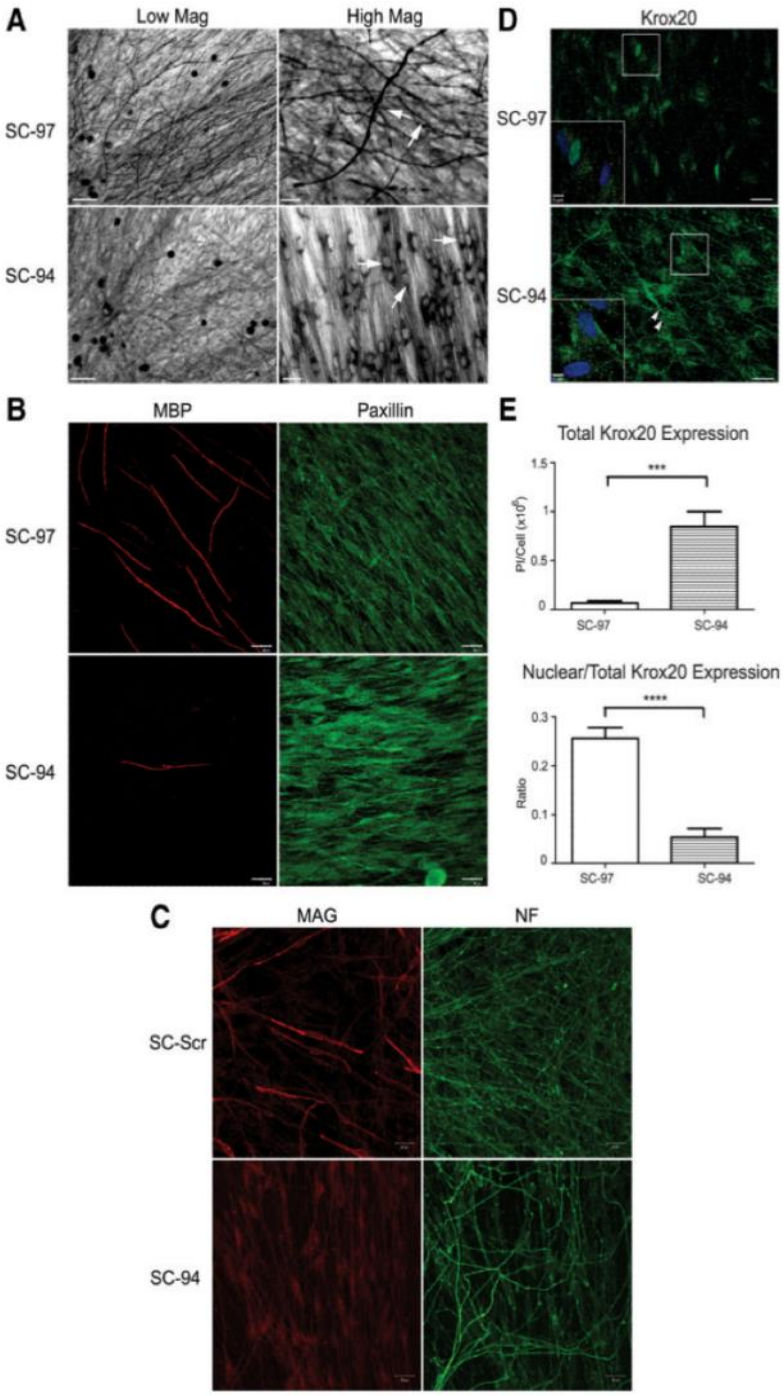

Figure 8. Cofilin is required for SC myelination.

(A) In four separate experiments, DRGN/SC co-cultures were assessed for myelination by Sudan black staining after 10–14 d of growth in myelin-permissive medium. SC-97 (top) robustly myelinated sensory axons, whereas SC-94 (bottom) myelinated very infrequently. At higher magnification (right), SC-94 cell shave rounded nuclei rather than oval nuclei as is typical for myelinating SCs. The oval nuclear shape of myelinating SC-97 is somewhat obscured but is visible in the cells indicated with arrows. Co-cultures grown for 10 d in myelination-permissive medium were also immunostained for MBP, MAG, paxillin,

neurofilament (NF), and Krox-20 expression. (B) SC-97 cell sproduced MBP-positive myelin segments with normal appearance; however, some SC-94 cells expressing higher cofilin levels produced occasional MBP-segments that were abnormally thin and short. (C) A subpopulation of SC-SCR (expressing scrambled shRNAi) cells expressed MAG and incorporated it into normal-appearing myelin segments, whereas all SC-94 cells expressed low levels of MAG that was not assembled into myelin. (D) Single-plane images of DRGN/SC co-cultures are shown. Krox-20 was expressed in the nuclei of SC-97 cells with only limited expression in the perinuclear region (inset). In contrast, Krox-20 immunoreactivity in SC-94 cells was largely cytoplasmic (see arrowheads), even extending into processes with low levels present in the nucleus (inset). DAPI-stained nuclei are shown in blue. (E) Quantification of total Krox-20 intensity and ratio of nuclear/total intensity normalized to the number of nuclei (mean of 5 Z stacks with 7–11 slices using a 0.5 μm interval). SC-94 cells expressed more Krox-20 than SC-97 cells, but it is predominantly localized in the cytosol. ***$p < 0.001$, ****$p < 0.0001$. Scalebars: A, low magnification, 50 μm; high magnification, 20 μm; B, C, D, 20 μm; inset in D, 5 μm.

Table 1. Quantification Of Sudan Black-Stained Myelin Segments

Experiment	Cell Type	N*	Mean ± SEM	% Decrease	*p* value
1	SC-97	4	184 ± 33	85	0.0005
	SC-94	6	27 ± 7		
2	SC-97	6	12 ± 4.6	90	0.039
	SC-94	6	1 ± 0.6		
3	SC-97	16	1095 ± 96	98	0.0001
	SC-94	14	15 ± 5		

*Number of DRGN/SC co-cultures examined

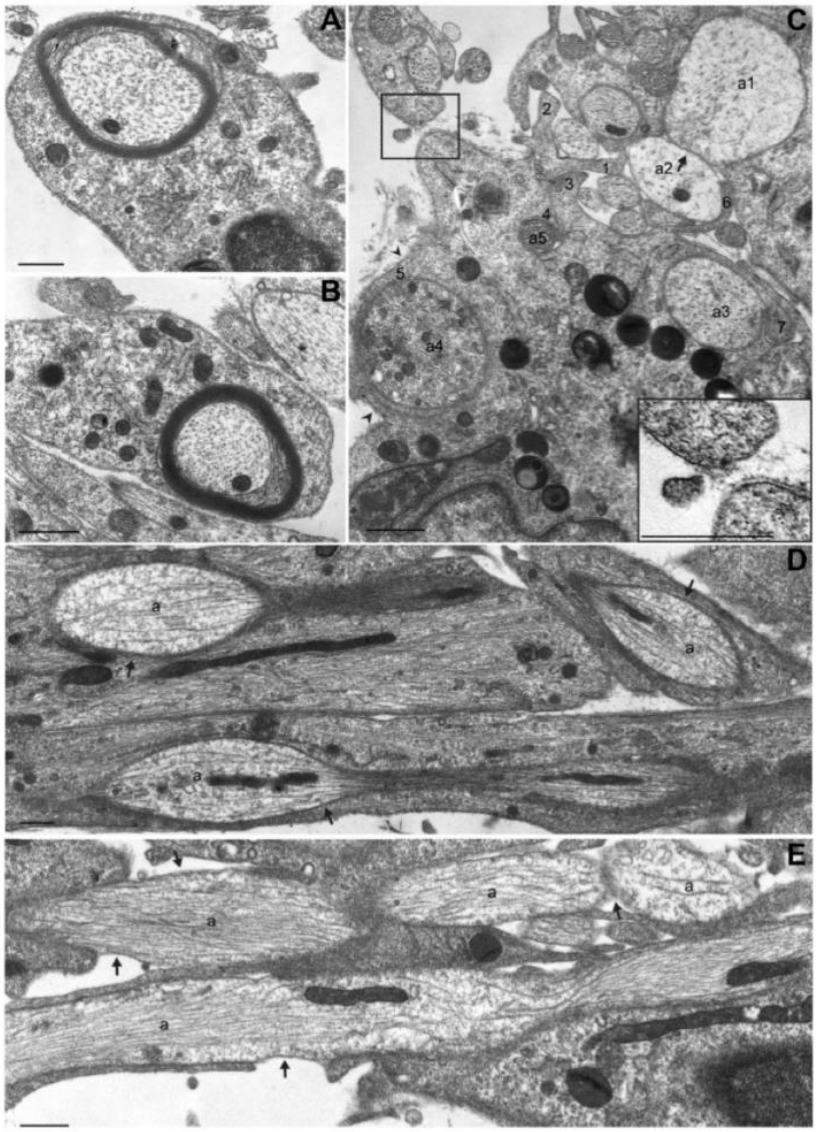

Figure 9. Cofilin is necessary for normal SC–axon interactions.

(A–E) Ultrastructural analyses were conducted on cross (A–C) and *en face* sections (D, E) of DRGN/SC co-cultures grown for 10 d in myelin-permissive medium. Where as WTSCs (A) and SC-97 cells (B) produced normal-appearing myelin within this time frame, SC-94 cells (C) did not. Large-diameter axons were not effectively segregated by SC-94 (axons a1, a2). SC-94 did not form a one-to- one relationship with axons, but rather elaborated multiple processes around both large- and small-diameter axons. Numbers indicate separate processes from a single SC-94 cell attempting to wrap two larger axons and multiple small ones (a3–a5). Arrowheads and the inset show discontinuous basal lamina (C). *En face* sections show that SC-97 processes formed tight appositions with axons (D, arrows), where as SC-94 processes did not adhere well to axons (E, arrows). Scale bars: 1 μm.

Table 2. Number Of DAPI-Stained SCs in DRGN/SC Co-cultures

Experiment	Cell Type	N*	Mean ± SEM	*p* value
1, M10d	SC-97	10	178 ± 10	0.1029
	SC-94	10	153 ± 10	
2, M10d	SC-97	20	75 ± 2	0.1258
	SC-94	20	100 ± 10	
3, CB1d	SC-97	24	122 ± 16	0.4125
	SC-94	24	108 ± 7	

*Total number of fields; M10d, co-cultures grown for 10 d in myelination feed; CB1d, co-cultures seeded with SCs for 1 d.

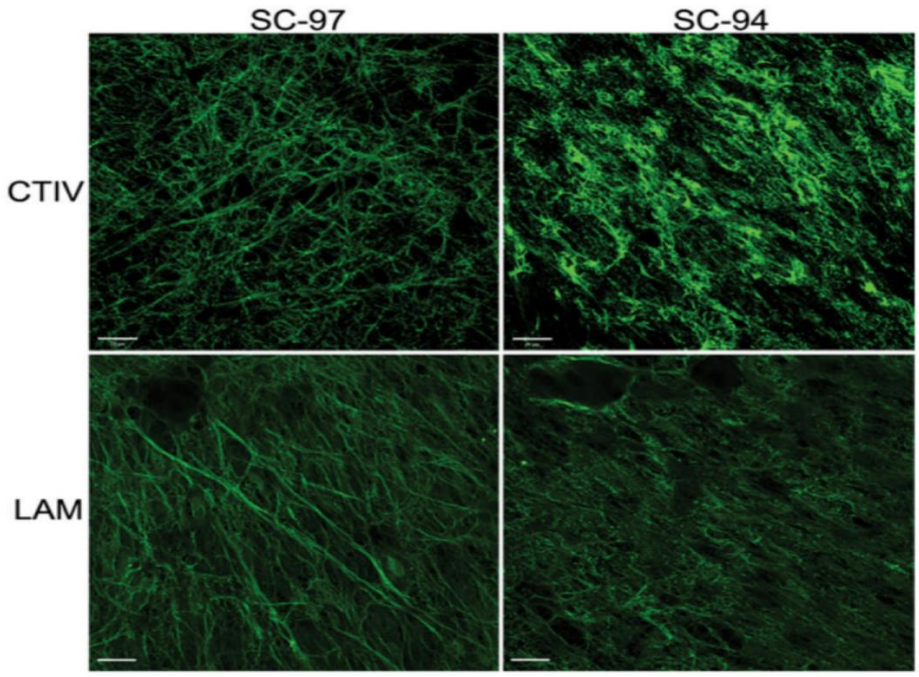

Figure 10. Cofilin-deficient SCs assemble an atypical extracellular matrix.

We assessed the ability of SC-94 to secrete and assemble basal lamina components by immunostaining DRGN/SC co-cultures grown for 10 d in myelination-permissive medium with antibodies to CTIV and LAM. Co-cultures were not permeabilized before immunostaining. CTIV was expressed by SC-97 and was assembled into linear arrays, whereas CTIV was expressed by SC-94 at high levels but was organized in patches throughout the co-culture. Laminin was secreted and assembled into linear arrays in SC-97 co-cultures, whereas it had an irregular distribution in SC-94 co-cultures. Images are maximum intensity projections of 10 Z series collected at 0.4 μm intervals. Scale bars: 20 μm.

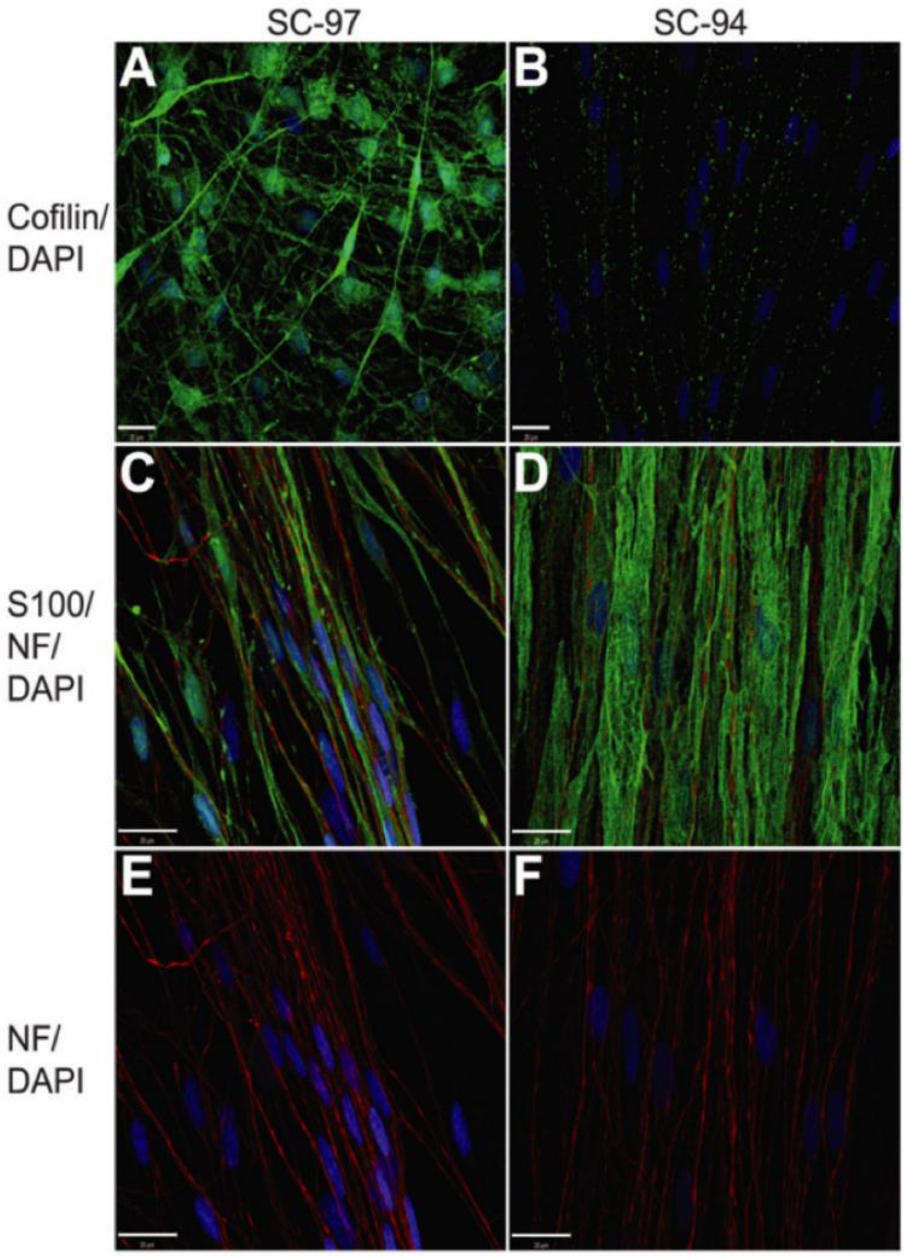

Figure 11. Cofilin-deficient SCs do not engage axons.

We used S100 and neurofilament immunostaining to examine the interaction between cofilin-deficient SCs and axons in DRGN/SC co-cultures grown for 10 d in myelination-permissive medium. We also tested for cofilin expression to verify that cofilin levels remained low in SC-94. Images are single planes. A, Cofilin was expressed by SC-97 and localized throughout the SC and its bipolar processes. B, Cofilin levels were reduced in SC-94 co-cultures. C, D, Similar areas of SC-97 and SC-94 co-cultures are shown. S100-positive SC-97 (green) aligned on axons (red), whereas SC-94 adhered to the laminin substrate and spread into large bipolar cells. However, SC-94 extended plasma membrane around axons that contacted their surface. E, F, Neurofilament and DAPI staining of the fields shown in B are presented. Scale bars: 20 μm.

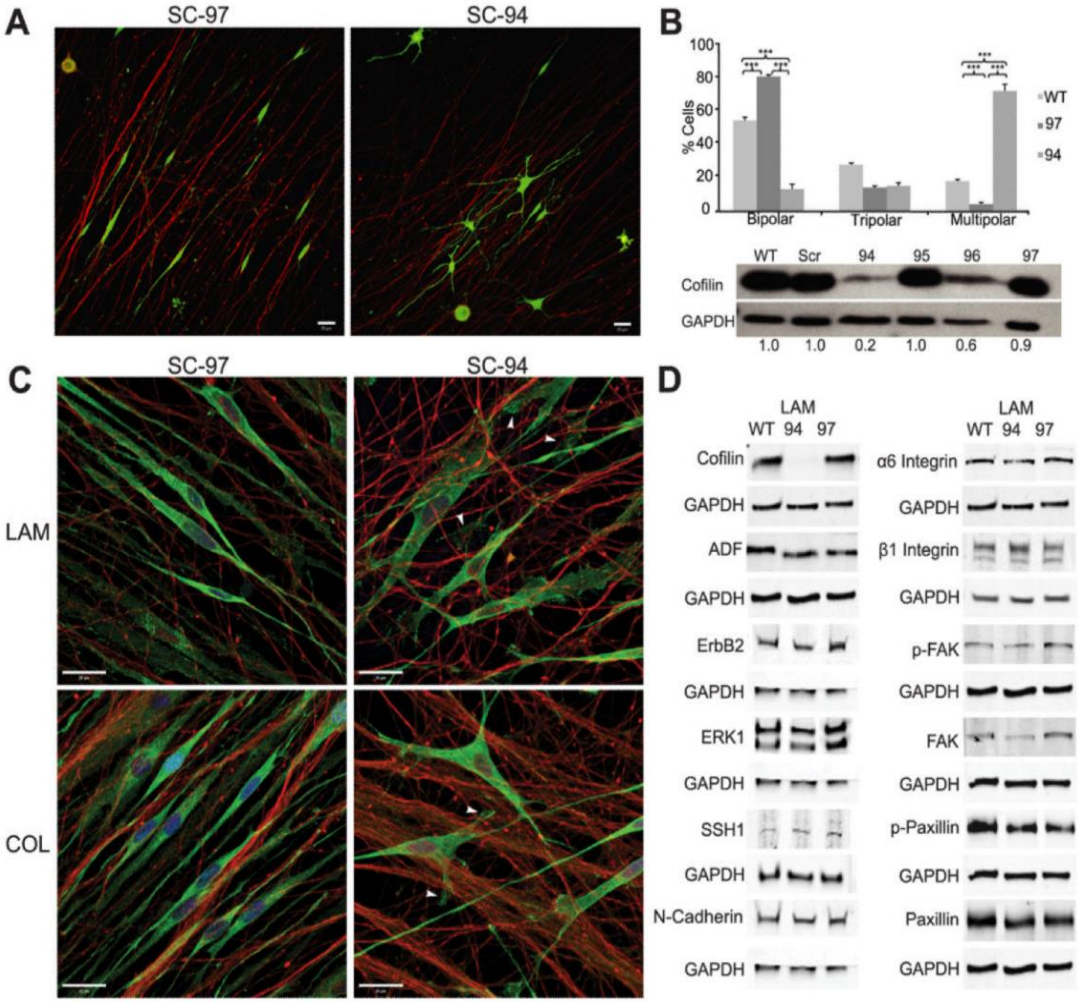

Figure 12. Cofilin is required for alignment of SCs on axons.

(A) Representative single-plane images of the morphology of CTG-labeled SC-97 (10% cofilin knockdown) and SC-94 cells (80% cofilin knockdown) is shown 24 h after seeding onto neurons (immunostained with neurofilament; red). SC-94 cells did not assume a bipolar morphology and did not align with the axons. (B) Quantification of cell morphology of SC-94 and SC-97 cells is shown. Eighty percent of SC-94 cells exhibited a multipolar morphology, while <20% of WT SCs and SC-97 cells were multipolar. The cofilin levels of SC-94 and SC-97 cells were measured by Western blot analysis. ***$p < 0.001$. (C) SC-97 and SC-94 lines were co-cultured with DRGNs grown on two different substrates, LAM and collagen (COL). Forty-eight hours after seeding onto neurons, co-cultures were fixed, and neurons were immunostained with neurofilament (red) and SCs with vinculin (green) to visualize SCs and focal adhesions. Images are single planes of representative areas. SC-94 cells were unable to assume a bipolar morphology and align along neurons grown on either substrate. (D) Total protein extracts of WT SCs and SC-97 and SC-94 cells grown normally for 48 h on LAM were blotted for basal levels of adhesion molecules (integrins, N-cadherin) and other downstream signaling molecules. Cofilin deficiency did

not correlate with an aberrant expression of other proteins, and viral transduction had no effect on expression levels of the tested proteins. Scale bars: 20 μm.

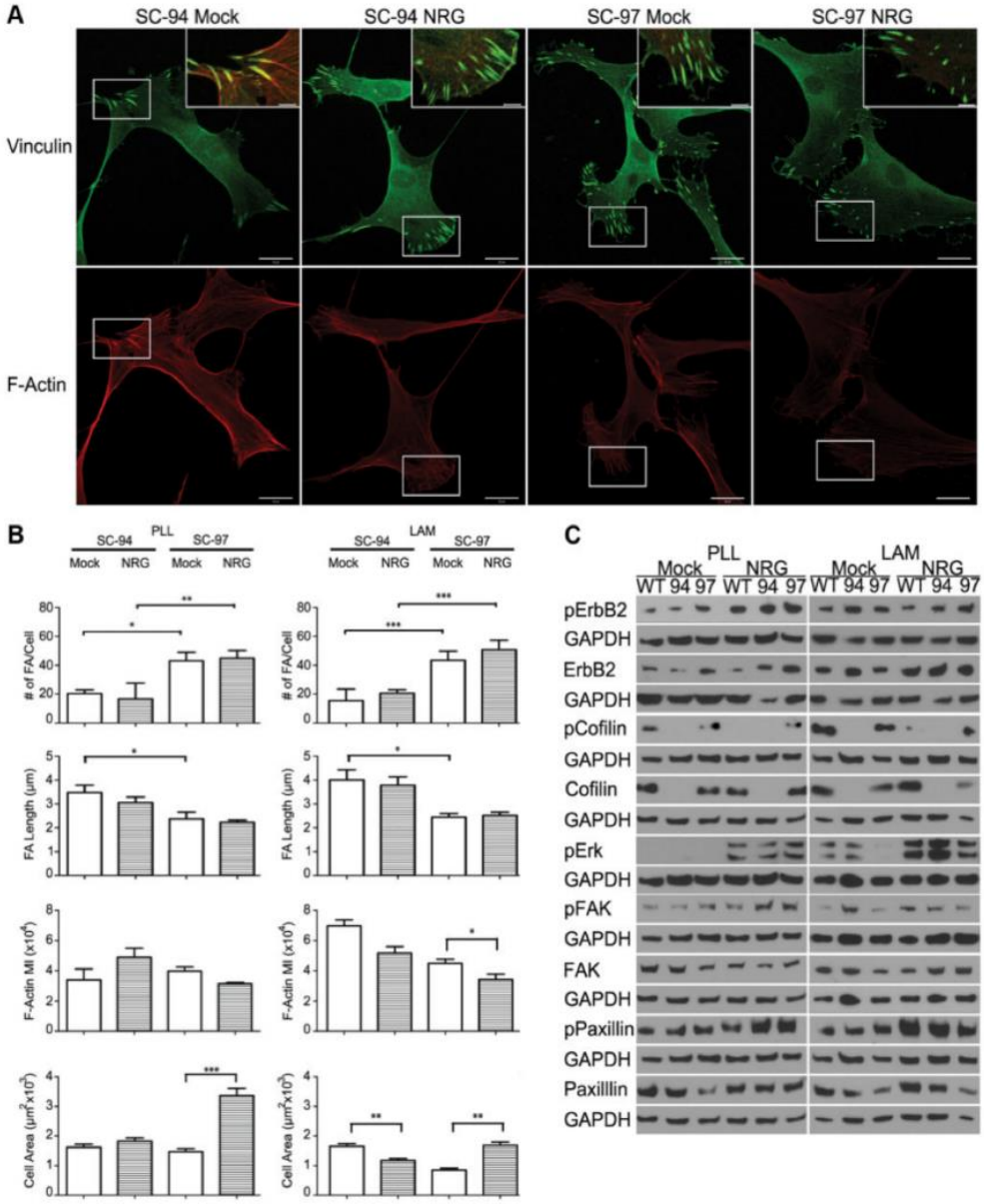

Figure 13. Cofilin-deficient SCs do not increase in size in response to NRG1.

Subconfluent SC lines grown on PLL and PLL/LAM were starved and stimulated with NRG as described in Figure 1. A, SC lines grown on LAM were immunostained with antibodies to vinculin (green) and stained with phalloidin (red) to visualize focal contact/adhesions and F-actin, respectively. Scale bars: 20 μm; inset, 5 μm. B, Quantification of the number and length of FAs per cell, mean pixel intensity of phalloidin, and cell area are shown. SC-94 cells had fewer but longer FAs than SC-97 cells. SC-94 cells did not respond to NRG1 stimulation on PLL, or decreased in cell size after stimulation LAM, while SC-97 cells showed a significant increase on both substrates. Three independent experiments were

analyzed. *p < 0.05; **p < 0.01; ***p < 0.001. C, Western blot analysis of 30 min NRG-stimulation assays of subconfluent WT SCs and SC-94 and SC-97 cells grown on PLL or LAM culture dishes are shown. No significant differences in protein phosphorylation were observed for SC-94 cells with respect to the controls.

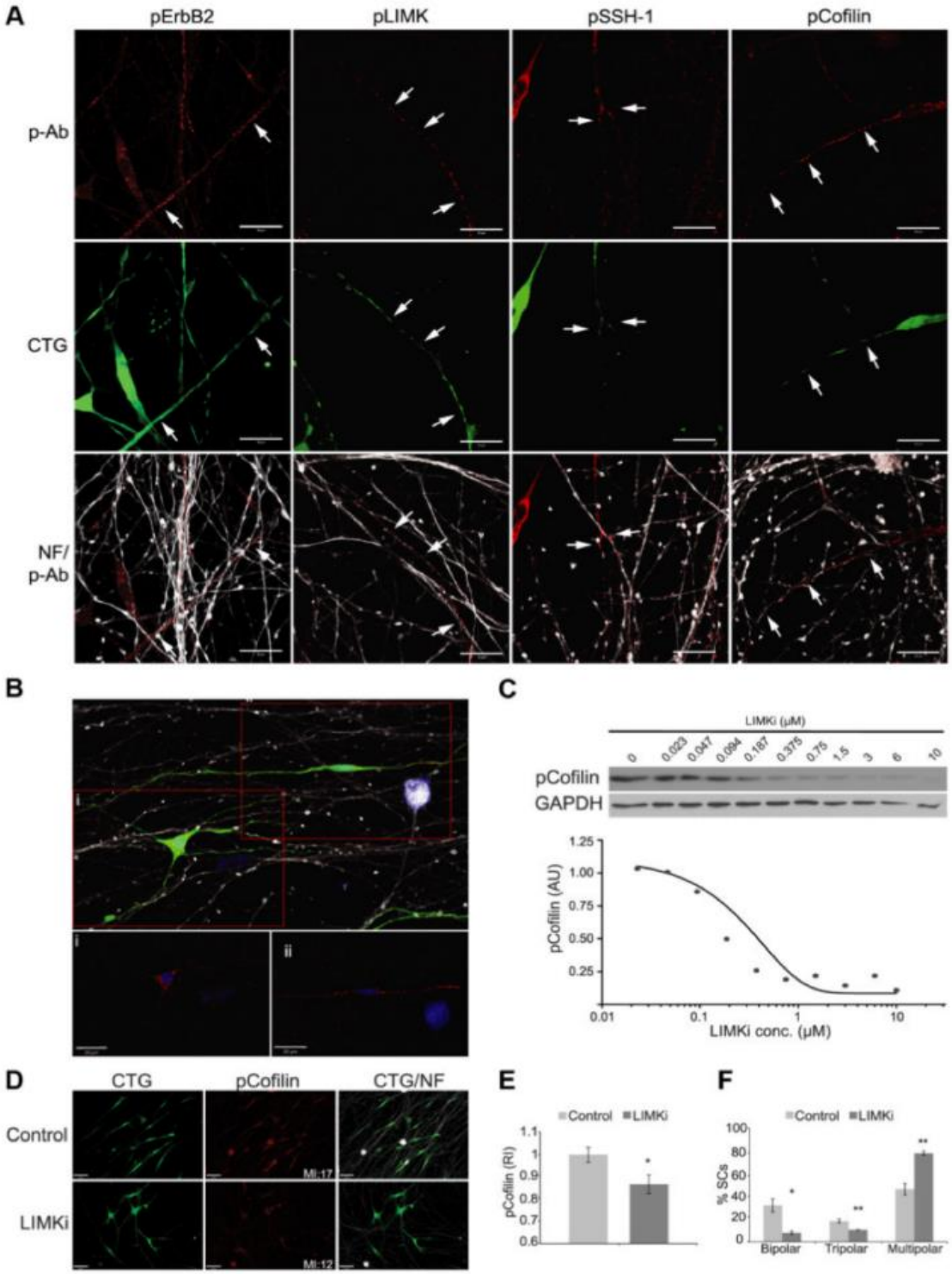

Figure 14. Cofilin S3 phosphorylation is necessary for SC alignment on axons. DRGN cultures were seeded with CTG-labeled WT SCs.

Co-cultures were fixed 24 h later and immunostained with antibodies to phosphorylated ErbB2, cofilin, LIMK, and SSH1 (all shown in red) and neurofilament (NF; white) to visualize axons. All Images are single planes optimized for each antibody. A, Phosphorylated forms of cofilin, LIMK, and SSH1 are present in the bipolar processes of SCs aligned along axons (arrows indicate protein in axon-aligned SCs). B, A single image of co-cultures reveals pS3-cofilin is present in processes of bipolar, aligned WTSCs, but not in those of multipolar SCs (insets i, ii). Only pS3-cofilin expression in the SC is shown. C, BMS-5, a LIMK inhibitor (LIMKi), inhibits cofilin phosphorylation in a dose-dependent manner. WT SCs were incubated for 4 h with serial dilutions of the inhibitor, and total cell extracts were assessed for pS3-cofilin levels and GAPDH as a loading control. The expression level of pS3-cofilin relative to GAPDH expression is plotted as a function of BMS-5 concentration. D, Representative images of a 24 h axon alignment assay conducted with SCs grown in the absence (DMSO control) and presence of 1 μM BMS-5 (LIMKi) and pS3-cofilin (red) is shown. The mean pixel intensity (MI) for pS3- cofilin in the image shown is provided. E, Quantification of pS3-cofilin immunofluorescence for the experiment shows a statistically significant reduction in pS3- cofilin in LIMK inhibitor-treated cultures compared to controls (mean ± SEM; 30 fields per condition). F, Quantification of SC morphology reveals fewer bipolar, aligned WT SCs in co-cultures grown in the presence of LIMKi than in controls. A graph of a representative experiment of three is shown with mean ± SEM. *$p < 0.05$; **$p < 0.01$. Scale bars: 20 μm.

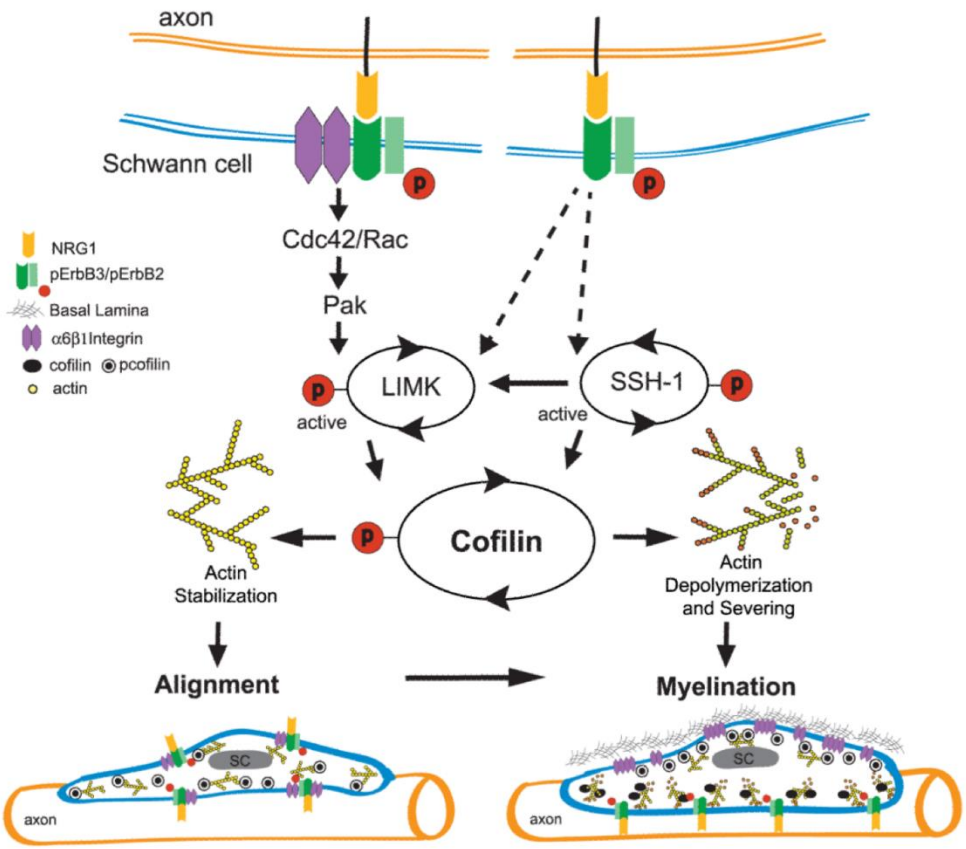

Figure 15. Working model for cofilin function during Schwann cell myelination.

We propose that the spatiotemporal balance of cofilin serine 3 phosphorylation and dephosphorylation regulates actin polymerization dynamics downstream of ErbB2/B3 and β1 integrin signaling in Schwann cells contacting axons. Schwann cell alignment on axons is facilitated by shifting the balance toward cofilin serine 3 phosphorylation that favors F-actin stabilization. In the absence of significant basal lamina deposition, α6β1 integrin and ErbB2/B3 receptors exist as a complex throughout the Schwann cell plasma membrane. Clustered β1 integrins activate Cdc42/Rac-dependent-Pak kinase (Thaxton et al., 2008) that increases LIMK- dependent phosphorylation of cofilin serine 3. As basal lamina develops, the receptors become polarized to opposing plasma membranes. Basal lamina clusters α6β1 integrin to promote cofilin serine 3 phosphorylation and stabilization of F-actin along the abaxonal plasma membrane. In contrast, NRG1 activation of ErbB2/B3 along the adaxonal plasma membrane inhibits LIMK and promotes SSH1 activity, which shifts the balance toward cofilin serine 3 dephosphorylation. Cycles of cofilin phosphorylation and dephosphorylation at the leading edge of the inner mesaxon allow expansion of the Schwann cell plasma membrane around the axon during active myelination.

CHAPTER THREE: MERLIN MODULATES NEUREGULIN-COFILIN SIGNALING DURING SCHWANN CELL MYELINATION TO ESTABLISH MYELIN SEGMENT LENGTH

Introduction

Schwann cells form the multi-lamellar myelin sheath surrounding axons in the peripheral nervous system (PNS). During nerve development, Schwann cells (SCs) migrate along axons and sort them according to diameter by extending and retracting lamellipodia-like protrusions either in parallel or perpendicular (radial) to axons (Jessen and Mirsky, 2005; Pereira et al., 2011). Once SCs establish a 1:1 relationship with the axonal domain destined for myelination, and basal lamina is present, they begin to synthesize new membrane and myelin proteins while simultaneously driving their expanding adaxonal membrane (that which touches the axolemma) repeatedly around the axon to generate the myelin sheath. Underlying these processes is the spatial-temporal regulation of actin filament assembly and disassembly by actin polymerizing/depolymerizing proteins. Control of actin dynamics needed for SC myelination remains poorly understood (Fernandez-Valle et al., 1997).

Recently we showed that cofilin, a member of the small (18kDa) actin depolymerizing factor family, is essential for SC myelination (Sparrow et al., 2012). Cofilin enables effective engagement of SCs with axons, and its activity is

regulated by a key molecule stimulating peripheral myelination, axonal-bound neuregulin1-type III, that activates the receptor tyrosine kinases (RTKs) ErbB2/ErbB3 in SCs (Michailov et al., 2004; Taveggia et al., 2005). Cofilin severs F-actin to achieve two functions. The first is to replenish the pool of G-actin monomers available for incorporation into growing actin filaments, and the second is to create barbed ends for nucleation of new F-actin branches (Bravo-Cordero et al., 2013). Its activity is regulated in several ways, but the best characterized is by phosphorylation/dephosphorylation on serine 3. LIM domain kinase (LIMK) phosphorylates S3-cofiin and decreases its actin severing activity by inhibiting cofilin's ability to associate with F-actin (Moriyama et al., 1996). LIMK is phosphorylated and activated by Rac/p21-activated kinase (PAK) (Edwards et al., 1999). LIMK can also be phosphorylated and activated by Rho-associated kinases (ROCK) and the myotonic dystrophy kinase-related Cdc42-binding kinase (MRCK) (Manetti 2012). Slingshot (SSH) is the major phosphatase that dephosphorylates S3-cofilin, leading to activation of cofilin. SSH activity is regulated by phosphorylation on S978 by PAK, which inhibits its ability to dephosphorylate and activate cofilin (Huang, et al. 2006).

Mutations in the *Nf2* gene result in the disorder Neurofibromatosis Type II (NF2), which predisposes individuals to formation of schwannomas on cranial and peripheral nerves (Petrilli and Fernandez-Valle 2016). The tumor suppressor merlin (also known as schwannomin), encoded by the *Nf2* gene, regulates both Rac (Morrison et al., 2007) and PAK (Kissil et al., 2003). Merlin is a member of the

FERM domain containing, 4.1 superfamily of proteins that link the actin cytoskeleton to membrane receptors, and regulates both growth and proliferation signaling pathways as well as those regulating actin dynamics. Cultured human schwannoma cells exhibit excessive Rac-associated membrane ruffling, and increased levels of both F-actin and focal adhesions (Pelton et al., 1998; Zhou et al., 2011). Merlin's activity is regulated by phosphorylation on S518 by protein kinase A (PKA) (Alfthan et al., 2004) and PAK (Kissil et al., 2002), which decreases its tumor suppressor activity. We previously demonstrated that in SCs specifically, merlin is phosphorylated on S518 by protein kinase A (PKA) downstream of ErbB2/ErbB3 activation, and by p21-activated kinase (PAK) downstream of B1 integrin activation (Thaxton et al., 2008).

A role for merlin in regulation of SC myelination has been suggested by several in vivo studies. Mice with a SC-specific inactivation of merlin form schwannomas, and exhibit a mild dysmyelinating phenotype, including SC hyperplasia, decreased internodal length, and paranodal defects (Giovannini et al., 2000; Denisenko et al., 2008). Conversely, we showed in an in vitro study that myelin internode length was significantly increased when wild type merlin was overexpressed at the time of myelination induction in DRG neuron/SC co-cultures, further suggesting that merlin plays a role in controlling the ultimate length of the myelin sheath (Thaxton et al., 2011).

Here we report that merlin indirectly suppresses LIMK activity downstream of neuregulin signaling allowing for activation of cofilin, and ultimately influencing myelin internodal length. Schwann cells with loss of merlin function migrate on and align with axons as well as differentiate and express myelin basic protein when grown in myelin-permissive conditions. However, merlin-deficient SCs form short myelin segments and do not activate cofilin in response to neuregulin. These studies suggest a role for merlin as an upstream regulator of cofilin activity during peripheral myelination.

Materials And Methods

Materials And Antibodies

Mission shRNA lentiviral transduction particles targeting human merlin, control non-target (scrambled) shRNA transduction particles, and puromycin were purchased from Sigma-Aldrich (St. Louis, MO). 2.5S nerve growth factor (NGF) was purchased from Harlan (Indianapolis, IN) and recombinant human neuregulin1-type III-SMDF (NRG) was purchased from R&D Systems (Minneapolis, MN). Antibodies for the following proteins were purchased from these sources: GAP43, merlin, neurofilament-heavy chain, PLP, Sox10 from Abcam (Cambridge, MA), S100 from Dako (Denmark), Cofilin-1 from Novus (Littleton, CO), pS3-cofilin-1, LIMK1, pT505/508-LIMK1/2, β-Actin, YAP from Cell Signaling (Davers, MA), MBP from Covance (Princeton, NJ), ErbB2, pY1248-ErbB2 from Santa Cruz Biotechnology (Santa Cruz, CA), Paxillin from BD

Biosciences, Rac-GTP from New East Biosciences, DAPI, Alexa Fluor conjugated secondary antibodies, Alexa Fluor 633-phalloidin from Life Technologies (Grand Island, NY), O4 and P0 were kind gifts of Dr. Paula Monje (University of Miami). . All cell culture reagents were purchased from Life Technologies unless otherwise stated. The LIMK inhibitor BMS-5 ($C_{17}H_{14}Cl_2F_2N_4OS$) was purchased from Synkinase.

Preparation And Culture Of Rat Primary SCs

Primary rat SCs were isolated from sciatic nerves of 8-12 two-day-old Sprague Dawley (Charles River, North Wilmington, MA) pups and prepared using the Brockes method with modifications as described (Brockes et al., 1979). Nerves were cleaned of connective tissue and blood vessels, and then digested by submersion in PBS with 1mg/ml collagenase for 20min, followed by 0.25% trypsin for 20min. Enzymes were inactivated twice with D10 (DMEM, 1x Pen/Strep, with 10% heat inactivated fetal bovine serum (HIFBS, Atlanta Biological, Atlanta, GA)) and centrifugation at 1500rpm for 5min at 4ºC. To obtain a single cell suspension, nerves were disassociated manually by triturating with small bore Pasteur pipettes. The single cell suspension was then plated into an uncoated, polystyrene Corning 60mm in D10 and cultured at 37ºC and 7% CO_2. To purify the culture, 18-24hrs later culture medium was changed to D10+1mM Ara-C for two days, and then again for another three days. On the seventh day post dissection, cultures were further by Thy1.1 incubation followed by guinea pig complement treatment. The remaining cells were then plated into a 200µg/ml Poly-L-Lysine (PLL; Sigma, St Louis, MO) coated 100mm dish in D10M medium (D10 with 2µM forskolin (Sigma,

St Louis, MO) and 20µg/ml pituitary extract (BTI, Stockbridge, MA)). Purified rat Schwann cells were routinely cultured on PLL-coated dishes in D10M at 37ºC and 7% CO_2, fed twice a week, split 1:3 when they reached 95-100% confluency, and used until passage 20.

Generation Of Merlin Deficient Schwann Cell Lines

shRNA target-45 (Sigma Mission) against human *NF2*/merlin mRNA has a 100% alignment to rat merlin mRNA and yielded a 95% reduction in merlin levels. Merlin-deficient SCs were generated in a similar manner to that of the Coflin-deficient SCs as previously described (Sparrow *et al.*, 2012). Briefly, freshly purified rat SCs were plated onto PLL-coated 6-well dishes and were cultured in D10M at 37ºC and 7% CO_2. When the cultures reached 70-80% confluency, lentiviral transduction particles were added at a multiplicity of infection (MOI) of 5 in D10M plus 8µg/ml hexadimethrine bromide (Sigma, St Louis, MO). After 18-20 hours, the infection medium was replaced with D10M for 24 hours, at which time culture medium was changed to D10M containing 1µg/ml Puromycin (Sigma, St. Louis, MO). SCs were maintained in D10M plus puromycin and were passaged to expand the population. During expansion, the merlin expression level was assessed by extracting SCs directly in SDS-PAGE sample buffer and conducting western blot analysis. SCs expressing scrambled (SCR) shRNA, along with untransduced, primary SCs, were used to control for the effects of lentiviral transduction, puromycin selection and passage number. Two independent merlin KD-SC lines were created and both had a similar reduction in merlin levels.

Preparation Of Rat Disassociated DRG Neuron/SC Co-Cultures

Dorsal root ganglia (DRG) were harvested from Sprague Dawley rat embryos at 15 - 17 days of gestation (E15-E17) and were dissociated in 2mL of 0.25% trypsin, in a 35mm petri, for 20min in the incubator. Enzymes were inactivated and removed with CB10 (MEM with 10% HIFBS) was used. Dissociated DRG neurons (DRGN) were plated at 0.2 ganglion per well in PLL (200µg/ml) and laminin (50µg/ml) coated 96-well plates with black sides in a total volume of 100µl CB5 medium (MEM, 0.4% glucose, and 50ng/ml 2.5S NGF, 5% HIFBS). They were placed in EF2 medium (CB with 1x N2 supplement, and 200µM FUDR & uridine (Sigma, St. Louis) 16-20hrs post seed for three days, and then maintained in CB5 for one week. Cultures were fed three times during this period. DRGN cultures were then seeded with either primary, scrambled control, or merlin-KD rat SCs at $25x10^3$ SCs per well in CB10 medium (CB with 10% HIFBS). One week later, co-cultures were switched to myelin-permissive medium M-feed (CB with 15% FBS, 0.05mg/ml L-Ascorbic acid), and fixed 10-14 days later and immunostained.

Immunofluorescence Staining And Imaging

SC Culture. Following two washes (3min) in PBS on ice, cultures were fixed with cold 4% paraformaldehyde in PBS on ice for 10min, permeabilized with 0.1% TX-100 in PBS for 10min at RT, and blocked for one hour in 10% normal goat serum in PBS (Block). Primary antibodies were diluted in Block and cultures were incubated at RT for one hour. Cultures were washed 3x for 10min with Block, and

secondary antibodies (goat-Alexa Fluor, Invitrogen) were applied for 30min at a 1:500 dilution in Block. Cultures were washed 3x for 10min with PBS. If applicable, DAPI (to stain nuclei) and/or Alexa-633-phalloidin (to stain F-actin) were added to the secondary antibody mixture. Finally, cultures were then mounted in Gel Mount (ECM Bioscience, CA, USA) and allowed to cure overnight in the dark. *Co-Cultures.* Co-cultures were stained similarly to SC-only cultures. Permeabilization was done with 0.3% TX-100 in PBS, Block buffer included 0.1% TX-100 which was also used for dilution of primary antibodies, and incubation was done overnight at 4°C. *Imaging.* All SC cultures were analyzed with a Zeiss LSM710 microscope and Zen 2009 software with 40x or 63x objectives. All co-cultures were imaged with a RunnerHD (Trophos). Conditions for image acquisition were optimized for each secondary antibody in stained cultures on separate channels, and the same conditions were used for acquisition of control and experimental cultures. Images are either single planes or maximum intensity projections as indicated in the figure legends. *Analysis.* Volocity 6.3 software (Perkin Elmer) was used to measure total well fluorescence and individual myelin segments, that were assessed by four different parameters: Mean Pixel Intensity of MBP (amount of MBP in segment; total pixel intensity divided by number of pixels in segment), Total Area of Myelin Segments (total number of pixels in segment), Shape Factor (a score of roundness where 0=straight line and 1=a circle), and Skeletal Length (true length of segment regardless of curve).

NRG Stimulation And Western Blot Analysis

SCs were seeded on 200µg/ml PLL-coated 6 well plates (Corning) at a density of 150-200x10^3 SCs/well and were grown until 70-80% confluency (72-96hrs) in D10M. Cultures were starved of serum and mitogens by rinsing twice in Hank's Balanced Salt Solution (HBSS, Gibco) and incubating in D0.5 (DMEM+P/S+0.5% HIFBS) for at least 24 hours prior to treatment. Duplicate wells per condition were treated for 30min at 37ºC and 7% CO_2 with either D0.5+vehicle (0.2% BSA in PBS, "Mock") or D0.5+30ng/ml NRG1-type III (SMDF, "Stim"). For stimulation in the presence of LIMK inhibitor BMS-5, cells were first preincubated with either 5µM BMS-5 or 0.05% DMSO, and subsequently stimulated in the presence of the drug or carrier for 30min at the same concentration. Following treatment, SCs were washed twice in cold PBS on ice and were extracted in 200ul (100ul/well) modified RIPA buffer+protease/phosphatase inhibitor cocktails (25mM Tris-HCl, ph 7.6, 150mM NaCl, 1% TX-100, 1% SDS, with 1x PIC, PIC2, PIC3 from Sigma) and then separated by SDS-PAGE as follows. 5-10ug of protein (protein concentration determined by DC Protein Assay, BioRad) from each lysate was loaded into a well of a pre-cast 15-well 4-20% polyacrylamide gels (HEPES buffered, Pierce). Proteins were transferred to PVDF membranes (Immobilon®-FL, Millipore). Membranes were blocked with a 1:1 Odyssey blocking buffer (Licor) and TBS (15.5mM Tris-HCl, 4.58mM Tris, 137.6mM NaCl) for either 1hr at room temperature or overnight at 4°C. Membranes were incubated with primary antibodies diluted in 1:1 Odyssey Block and TBS-T (TBS with 0.1% Tween-20) for either 1hr or overnight at 4°C with agitation. Following three 10 min washes in TBS-

T, membranes were incubated for 45min with IRDye (either 700 or 800) conjugated goat anti-mouse or anti-rabbit secondary antibodies (Licor) at 1:25,000 dilution in a 1:1 of Odyssey Block:TBS-TS (TBS-T with 0.02% SDS). Membranes were washed three times for 10 min each in TBS-T and quickly at least twice with TBS before scanning on a Licor Odyssey imaging system.

Developmental Studies

Western Blot. Sciatic nerves were isolated from rats at the indicated postnatal days, cleaned of extraneous tissue and flash frozen with liquid nitrogen. After thawing on ice, they were extracted by homogenizing in a glass tissue grinder in RIPA buffer (above) followed by sonication. Extracts were subjected to SDS-PAGE and blotted as above. *Immunofluorescence Of Teased Sciatic Nerve.* Cleaned sciatic nerves were fixed by submersion in 4% paraformaldehyde in PBS on ice for 30min, rinsed briefly in PBS, and stored at 4°C in PBS. Approximately 0.5mm pieces of nerve were carefully teased apart on Superfrost Plus Gold slides (ThermoFisher) using Dumont #5CO forceps in PBS. They were allowed to dry for 6hr-18hr in tissue culture hood, before staining and mounting as described fro myelinating co-cultures. Imaging was performed similarly to SC cultures.

Live Imaging, Motility, And Alignment Assays

Wild-type (WT), scrambled (SCR), merlin-knock down (MKD) rat SCs were lifted by incubation in 0.05% trypsin, labeled with 1µg/ml Hoechst 33342 for 45min at 37ºC/7% CO_2, and then seeded onto purified rat DRG explants grown on PLL

(200µg/ml) and Laminin (25µg/ml) coated Mat-tech 12-well plate with 10mm glass insert at 5000 cells per insert. They were immediately placed on a Zeiss wide field microscope with full incubation control. Three to four hours later, five fields were selected for each cell type and images were collected with a Hamamatsu ORCA camera every 10 minutes for 24 hours using a 10x phase objective and Zeiss AxioVision 4.8.2 software. Volocity 6.3 software (Perkin Elmer) was used to manually track cells by selecting the center of the nucleus of cells that remained within the field of view for 80% of the duration of the movie. Four parameters were measured: Length (total distance traveled), Velocity (speed along length), Displacement (shortest distance between position of cell in first and last frame), and the Meandering Index (Displacement/Length).

Statistical Analysis

Western blots were quantified using Licor Image Studio (v3.0). The integrated intensity of similar sized regions of interest for phosphorylated and total proteins were obtained and normalized to β-actin signals. All graphs show mean, standard error of the mean (SEM), and p-values (see figure legends for specific statistic test run) and were calculated using Prism 6 (GraphPad Software, Inc., La Jolla, CA).

Results

Merlin Deficiency In SCs Causes Changes In Morphology, Growth Factor Independent Proliferation, And Loss Of Contact Inhibition.

To investigate the role of merlin during myelination, we transduced primary rat SCs with merlin shRNAi to produce merlin knockdown cells (MKD-SC) and compared them to wild type (WT-SC) and scrambled shRNAi (SCR-SC) controls (Fig. 16A). A proliferation assay was performed over a 72-hour time period in which MKD-SC were grown in D10M (DMEM with 10% FBS, and forskolin, and SMDF) or D10 (DMEM with 10% FBS) (Fig. 16B). WT- and SCR-SC controls were grown in the standard D10M medium only. MKD-SC in D10M grew four times faster than control cells, whereas those grown in D10 grew at a similar rate as control SCs grown in complete medium. This result indicates that MKD-SC proliferation is independent of mitogens, but dependent on serum.

Furthermore, we observed that MKD-SC did not exhibit the typical bipolar morphology nor “swirling” behavior of normal SCs when they became confluent (Fig. 16C). They also lost contact inhibition of growth and formed aggregates similar to that of cultured schwannoma cells (Pelton et al., 1998; Zhou et al., 2011). At lower cell density they exhibited a phase-neutral, “flat” morphology and attached and spread more quickly, similar to cofilin-deficient cells (Sparrow et al., 2012). We next examined the expression of standard SC markers by immunofluorescence (Fig. 16D). Confocal images indicated that there were no significant changes in expression or subcellular localization of GAP43, PLP, P0, O4, Sox10, and YAP

except for localization of S100, where it was present in both the nucleus and cytosol in SCR-SC but was predominantly expressed in the nucleus in MKD-SCs.

MKD-SCs Overpopulate And Form Short Myelin Segments When Co-cultured With Neurons.

To determine if merlin was necessary for myelination, WT-, SCR-, and MKD-SC were co-cultured with disassociated DRG neurons in 96-well plates and then grown in myelination-permissive medium for 10-14 days. Co-cultures were fixed and immunostained for myelin basic protein (MBP), Neurofilament-heavy chain (NF-HC), and DAPI (Fig. 17A). Total well florescence was measured for each channel, and the values obtained were normalized to the WT signals (Fig. 17B). There was a significant increase in the number of cells in MKD-SC co-cultures, indicated by an increase in DAPI signal, compared to controls, but a similar amount of both NF-HC and MBP fluorescence. However, if the fluorescence of MBP is normalized to that of DAPI, then there is less MBP expression in MKD-SC co-cultures than controls.

To further characterize myelin formation, regions of interests were drawn around individual myelin segments (approximately 55 segments per condition) to assess myelin segment length and shape (Fig. 17C). The results indicate that although individual segments contained similar amounts of MBP, the myelin segments formed by MKD-SC were significantly rounder, shorter, and overall smaller compared to segments produced by control SCs. High magnification confocal

images of SCR- and MKD-SC co-cultures confirmed the length and shape differences in MKD-SC compared to controls (Fig. 17D). These data indicate that merlin influences the length of individual myelin segments.

MKD-SCs Migrate And Elongate On Axons, But Do Not Activate Cofilin Downstream Of Neuregulin Signaling.

To investigate why MKD-SC were unable to produce normal myelin segments, we first assessed their ability to interact with axons. We tracked motility of Hoechst-labeled WT-, SCR-, and MKD-SC within the first 24 hours of co-culture with DRG neurons, and then categorized their morphology at the end of this period to assess their alignment with axons. We measured four motility parameters: the length, velocity, displacement, and the meandering Index (Fig. 18A). We found no significant differences in any of the parameters between the merlin expressing and non-expressing SCs. Therefore, we concluded that the absence of merlin does not impair the ability of SCs to migrate along axons. Using the last frame of each movie, we categorized the morphology of each cell as either “bipolar”, indicating alignment with an axon, or “other” (uni- or multipolar), indicating the cell was unaligned with a single axon (Fig. 18B). We found that in each type of cell there were approximately 90% aligned, bipolar cells, demonstrating that merlin is not needed for SCs to elongate on axons, a prerequisite for myelination.

We previously demonstrated that cofilin’s actin-severing function is activated in WT-SCs within 30 minutes of stimulation with neuregulin (NRG) as evidenced by

a reduction in pS3-cofilin levels (Sparrow et al., 2012). To test if merlin was necessary for activation of cofilin by NRG, we starved sub-confluent WT-, SCR-, and MKD-SC of serum and mitogens for 24 hours, and then either mock-stimulated or stimulated them with NRG for 30 minutes. Total cell lysates were blotted for total and phosphorylated ErbB2 and cofilin (Fig. 18C) to assess the activation of both proteins. All SC types increased pY1248-ErbB2 levels in response to NRG stimulation; however, the increase in MKD-SC was nearly two-fold above control cells. This is consistent with published work that showed a higher expression of surface receptors in merlin-deficient SCs compared to WT-SCs (Lallemand et al, 2009a). Despite this robust stimulation, pS3-cofilin levels in MKD-SC increased rather than decreased as expected and observed in both types of control SCs.

To understand why NRG failed to activate cofilin in MKD-SC, we first assessed the basal level of Rac activity in the cells. Rac is both an upstream regulator of cofilin, as it causes activation of LIMK via its activation of PAK, and a target of merlin regulation (Morrison et al., 2007). In addition, we asked if MKD-SC had higher levels of F-actin, the end target in this signaling pathway, that would be consistent with an increase in the level of inactive pS3-cofilin (Fig. 18D). We observed an increase in both active Rac-GTP and F-actin levels in MKD-SC compared to control SCs indicating aberrant regulation of signaling proteins in the NRG-ErbB2/3-cofilin-actin pathway in the absence of merlin.

We hypothesized that the level of active pT508-LIMK would be higher in MKD-SC than in control cells based on our observation of increased Rac-GTP and F-actin levels, and our previous work that showed increased phosphorylated LIMK in both merlin-null cell lines and NF2 paitent samples (Petrilli et al., 2014). Thus, inhibiting the LIMK activity at the time of NRG stimulation should lead to dephosphorylation and activation of cofilin. Following a 30min pre-incubation with BMS-5, a LIMK1/2 inhibitor, we stimulated WT-, SCR-, and MKD-SC in the presence of BMS-5 or 0.05% DMSO (vehicle), and again assessed both pY1248-ErbB2 and pS3-cofilin levels (Fig. 18E). Whereas NRG promoted dephosphorylation of cofilin in control SCs regardless of LIMK inhibition, NRG promoted dephosphorylation of cofilin in MKD-SC only when LIMK was inhibited. This result is consistent with a role for merlin in inhibiting LIMK activity to allow cofilin activation in SCs downstream of neuregulin signaling.

Merlin, LIMK, SSH, And Cofilin Are Developmentally Regulated.

We examined the expression and activation levels of merlin, cofilin, LIMK, and slingshot phosphatase (SSH) during nerve development. Total protein lysates of rat sciatic nerves at postnatal days 1, 5, 15, and 90 were immunoblotted for total and phosphorylated proteins (Fig. 19A, B). Over time, total merlin levels remain constant, but phosphorylation of the major regulatory residue serine 518, which indicates inactivation of the tumor suppressor activity, peaked at postnatal day 15. This is the time of active myelination and decreasing SC proliferation. Total and phospho-threonine 508 LIMK (active LIMK), as well as total and phospho-serine 3

cofilin (inactive cofilin) levels increased over time. There was a near 3-fold increase in total LIMK and cofilin, and a 2-fold increase in the percent of pT508-LIMK (active), and a 3-fold increase in the percent of pS3-cofilin (inactive). Total SSH levels remained consistent, while there was a drastic 40-fold increase in the percent of pS978-SSH (inactive) levels. These data indicate that cofilin is active during earlier stages of peripheral nerve development when myelination occurs, and its activity is inhibited as SCs stabilize their cytoskeleton following myelination.

We also conducted immunofluorescence of teased P1, P15, and P90 rat sciatic nerves to spatially localize cofilin in SCs as they mature (Fig. 19C). P15 and P90 nerves were stained for myelin basic protein (MBP) to reveal mature SCs. The P1 nerve was immunostained for paxillin as MBP is not present at this time (Fig. 18A). Additionally, nerves were immunostained for neurofilament-HC (NF-HC) to reveal axons and with DAPI. At P1, cofilin is diffusely distributed in immature SCs associated with axons. At P15, cofilin is localized to the adaxonal membrane (inner mesaxon). At P90 cofilin is present both at the adaxonal membrane and in Schmidt-Lanterman incisures (SLI) in mature, MBP-positive SCs. The location of cofilin at the adaxonal membrane is consistent with the hypothesis that cofilin participates in promoting motility of the adaxonal membrane around the axon as SCs myelinate in response to axonal neuregulin signaling. These data demonstrate that cofilin is temporally and spatially regulated during PNS nerve development.

Discussion

Cofilin Is Localized To Facilitate Expansion And Wrapping Of The Schwann Cell Inner Mesaxon During Myelination.

Our previous and current study have shown that cofilin is dephosphorylated and activated by NRG in SCs (Fig. 18C; Sparrow et al., 2012). Cofilin has been shown to be activated by NRG in other cell types as well (Nagato-Ohashi et al., 2004). Moreover, we previously showed that NRG causes recruitment of cofilin to the plasma membrane and leads to an increase in SC size (Sparrow et al., 2012). Here we demonstrate that cofilin is localized to the adaxonal membrane in rat sciatic nerves by P15 when active myelination occurs (Fig. 19C). Cofilin may be localized to the adaxonal membrane by binding to phosphatidylinositol (4, 5)-trisphosphate (PIP2) (Bravo-Cordero et al., 2013), as PIP2 is enriched at the adaxonal membrane (Pereia et al., 2011). Binding to PIP2 inhibits cofilin's severing activity and localizes it to the plasma membrane. Both G-protein coupled receptor (GPCRs) and RTKs, such as ErbB2/ErbB3, can stimulate phospholipase C hydrolysis of PIP2 while cofilin is bound, releasing active cofilin from the plasma membrane to enable leading edge protrusion (Yin and Janmey, 2003). Furthermore, cofilin becomes hyper-phosphorylated in the sciatic nerve at later stages of nerve development (Fig. 19A, B), indicating inhibition of actin severing activity in mature nerves. This is consistent with stabilization of the actin cytoskeleton once SCs have established a mature sheath around the axon. Hence, this evidence supports the hypothesis that cofilin facilitates the expansion and

subsequent wrapping of the inner mesaxon during myelination to establish the multi-lamellar myelin sheath.

Merlin Indirectly Suppresses LIMK Activity Enabling Neuregulin-Induced Cofilin Activation.

In normal SCs, cofilin is dephosphorylated and activated in response to NRG (Sparrow et al., 2012; Fig. 18C). NRG also simultaneously promotes dephosphorylation of LIMK and SSH, leading to inactivation and activation of these cofilin regulating enzymes, respectively (Sparrow et al., 2012). Furthermore, we previously demonstrated that NRG antagonizes PAK activation by stimulating dephosphorylation of PAK (Thaxton et al., 2008). Taken together, this regulation of upstream signaling molecules would ultimately lead to a decreased pS3-cofilin level and increased actin severing needed for cell motility and dynamic changes in morphology.

Our results indicated that in the absence of merlin, SC are unable to activate cofilin downstream of NRG (Fig. 18C). Merlin is a well characterized suppressor of both Rac and PAK (Morrison et al., 2007; Kissil et al., 2003). Indeed, we show that in the absence of merlin, basal levels of active Rac and F-actin in SCs are increased (Fig. 18D). Thus the normal balance between active and inactive cofilin is disrupted in MKD-SC. Specifically, higher amounts of Rac-GTP would lead to active, phosphorylated PAK and LIMK, in turn leading to an increase in phosphorylated and inactive cofilin, and thus stabilized F-actin. Evidence for hyper-phosphorylated

LIMK and cofilin has been published in both mouse merlin null cells and human schwannomas (Petrilli et al., 2014). A higher basal level of LIMK activity in MKD-SC would counteract the ability of NRG to promote dephosphorylation and activation of cofilin. The ability of NRG to promote cofilin dephosphorylation in MKD-SC treated with BMS-5 is consistent with this conclusion (Fig. 18E). A potential signaling pathway by which merlin modulates NRG-ErbB2/3-cofilin signaling in SCs to facilitate myelination is presented (Fig. 20).

Merlin Establishes Myelin Segment Length.

A subpopulation of MKD-SC expressed MBP but formed only shorter myelin segments compared to control SC in co-cultures (Fig. 17C). This is in direct contrast to SC overexpressing merlin, which we previously showed elaborated very long myelin internodes (Thaxton et al., 2008). We propose that the short internodes observed in merlin-deficient SCs arise from fewer wraps around the axon due to attenuated motility and expansion of the adaxonal membrane because of the inability to activate cofilin downstream of NRG. With each wrap, both the length and thickness of the myelin sheath incrementally increase. If the expansion and motility of the inner mesaxon is abnormal due to dysregulation of cofilin, then the myelin internode would be both shorter and thinner than normal. In addition, every myelin layer must be anchored to the axolemma at paranodal contacts (Salzer 2003). These contacts have been shown to be interrupted in mice with conditional inactivation of the *Nf2* gene (Denisenko et al., 2008). Therefore, an alternative explanation for the short internodes observed *in vitro* is that the

expanding myelin membrane cannot anchor itself to the underlying axolemma in the absence of merlin. Our present data cannot definitively distinguish between these two possibilities.

In an earlier study, SC hyperplasia subsequent to merlin loss was proposed as a possible explanation for the short internodes observed in mice with conditional Nf2 inactivation (Denisenko et al., 2008). Three types of mutant merlin mice were analyzed: P0-SCH-Δ39-121, P0-SCH-ΔCter, and P0Cre;*Nf2*$^{flox2/flox2}$. The first two mutant strains had a SC-specific overexpression of two dominant negative forms of merlin, whereas the last had a SC-specific deletion of merlin. Only the P0Cre; *Nf2*$^{flox2/flox2}$ (merlin-null) had significantly shorter internodes, even after accounting for axon caliber. Similarly, we found both short internodes and SC hyperplasia in the MKD-SC/DRG neuron co-cultures. SC hyperplasia was due to the fast proliferation rate and mitogen independent growth of MKD-SCs. These findings suggest that SC hyperplasia alone is insufficient to cause short internodes and that merlin has an additional and separate role in controlling actin dynamics. Support for this conclusion is provided by published work that indicates that merlin's tumor suppressor role is separate from its role as an actin cytoskeleton regulator (Lallemand et al., 2009b). Overall, the current study suggests that merlin plays an essential role in establishing myelin length as it allows for cofilin activation downstream of NRG-ErbB2/3 signaling in myelinating SCs.

Figures

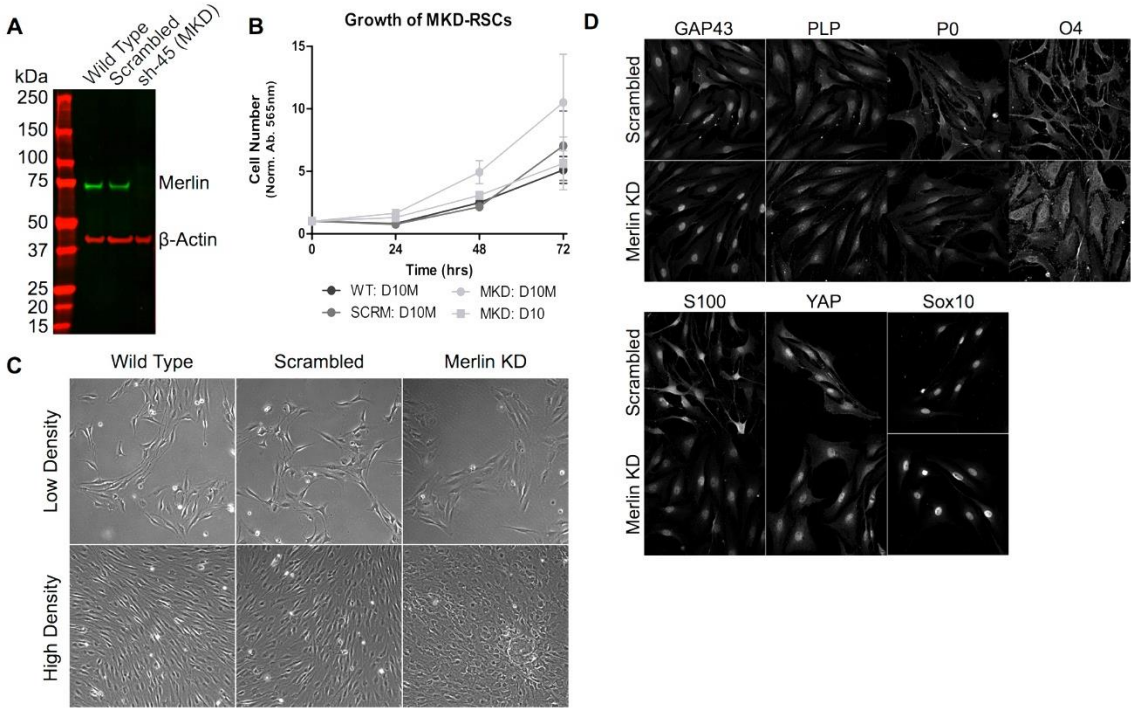

Figure 16. Primary rat Schwann cells with merlin-KD proliferate independently of mitogens, do not contact Inhibit and lose bipolar morphology.

Primary rat SCs (SCs) were transduced with shRNAi targeting either a random sequence (scrambled, or SCR) or merlin mRNA (shRNA-45, or MKD). (A) An immunoblot of total cell lysates shows shRNA-45 causes approximately 95% reduction of merlin levels compared to wild type (WT) RSCs. (B) Crystal violet growth assay performed over a 72-hour time period. MKD-SC were grown in either D10M or D10. WT and SCR controls were grown in D10M only. MKD-SC in D10M grew four times faster than control cells (n=2, 1 experiment each using one of two MKD-SC derivations; slopes of linear regression: WT=0.0075, SCR=0.0072, 45=0.030). (C) Phase contrast images of all three types of cells grown on PLL and in D10M at low and high density. (cell aggregates; arrow). (D) Confocal, single-plane, immunofluorescent images of SCR- and MKD-SC grown on PLL in D10M for the indicated SC marker proteins.

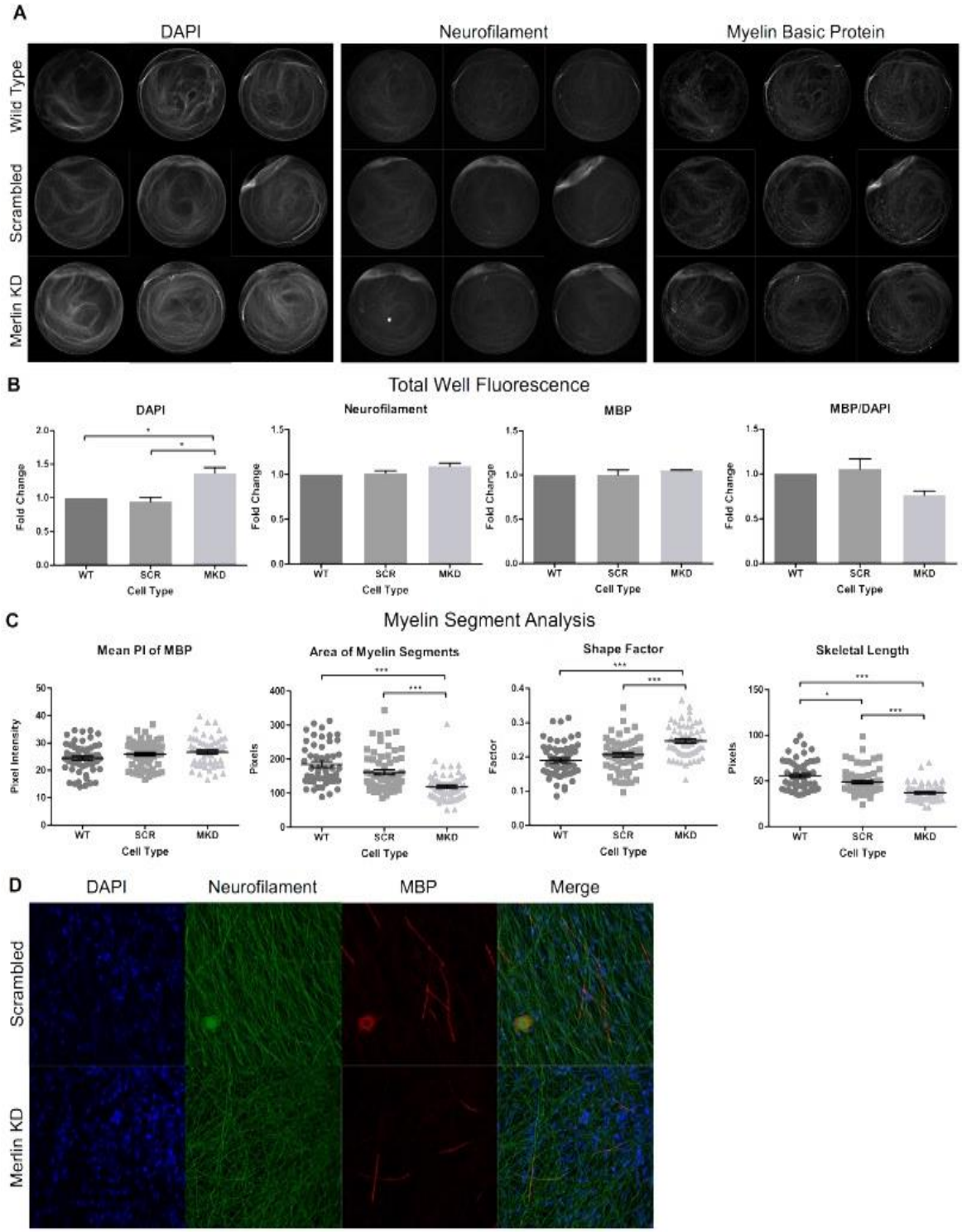

Figure 17. Merlin-KD SCs overpopulate and form short myelin segments *in vitro*.

WT-, SCR-, and MKD-SC were co-cultured with purified DRG neurons in ascorbic acid containing medium for 2 weeks to induce myelination and immunostained for myelin basic protein (MBP), Neurofilament-heavy chain (NF-HC), and DAPI. (A) Images of representative wells of myelinating co-cultures. (scale bar=diameter of well=6.39mm) (B)

Total well fluorescence for each channel from two independent experiments in which two independent MKD-SC derivations and their respective passage matched WT and SCR controls were used. Within each experiment 13-14 individual co-cultures were analyzed and averaged. The value for SCR- and MKD-SCs are reported as fold change where co-cultures containing WT-SC were set to one. Fold change values for the two experiments were averaged and graphed. (n=2, significance determined by one-way ANOVA, followed by Tukey's post test, *=p-value < 0.05). (C) Using Volocity software individual myelin segments were defined from a representative of two experiments, and four different parameters were compared: Mean Pixel Intensity of MBP (amount of MBP in segment), Total Area of Myelin Segments, Shape Factor (a score of roundness where 0=straight line and 1=a circle), and Skeletal Length. (n=50-58, significance determined by one-way ANOVA, followed by Tukey's post test, *=p-value < 0.05, ***=p-value < 0.001) (D) Single-plane, confocal images of SCR- and MKD-SC containing co-cultures confirm the shape and length difference between myelinating SCR- and MKD-SC.

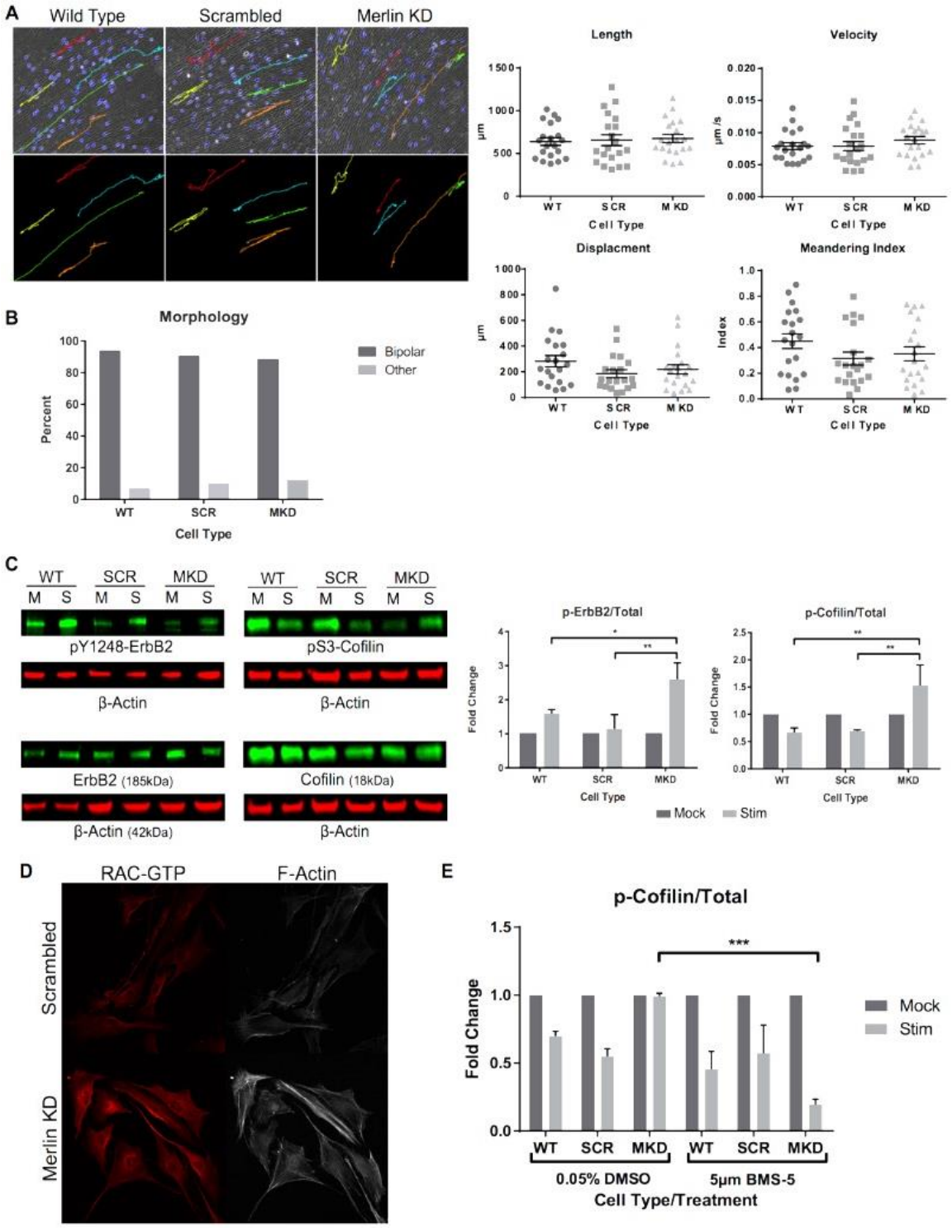

Figure 18. MKD-SC interact normally with axons, but fail to activate cofilin in response to neuregulin stimulation.

Hoechst labeled WT-, SCR-, MKD-SC were seeded on DRG neurons and imaged with full incubation once every 10 minutes for 24 hours. The first frame from a representative experiment is shown with 5 tracked cells. Arrowhead indicates direction of cell of

movement along the path. Twenty cells, remaining within the field of view for 80% of the duration of the movie, for each cell type were tracked. Four parameters were measured: Length (total distance traveled), Velocity, Displacement (shortest distance between position of cell in first and last frame), and the Meandering Index (Displacement/Length). (B) Morphology of 310-350 cells per cell type was assessed as either bipolor (aligned with axon) or other (multipolar, or unaligned with axon) approximately 27hrs after seeding on neurons. (C) Serum and mitogen starved WT-, SCR-, and MKD-SC were either mock stimulated (vehicle; M) or stimulated with NRG (S) for 30 minutes. Lysates were blotted for total and phosphorylated ErbB2 and cofilin. Results from three independent experiments (two MKD-SC derivations) were normalized to their respective β-actin, phosphorylated protein expressed as ratio of total protein, and normalized to mock condition. (n=3, significance determined by two-way ANOVA, followed by Tukey's post test;. * p-value < 0.05, ** p-value < 0.01). (D) Confocal, immunofluorescent images of SCR- and MKD-SC grown on PLL in D10M for active Rac (Rac-GTP) and F-actin. (E) WT-, SCR-, and MKD-SC were stimulated similarly to those in (C), but either in the presence of the LIMK inhibitor BMS-5 or vehicle (0.05% DMSO), and total cell lysates were blotted for total and pS3-cofilin. Measured signals from two independent experiments were averaged similarly as in (C) (n=2, significance determined by two-way ANOVA, followed by Tukey's post test;. *** p-value < 0.01).

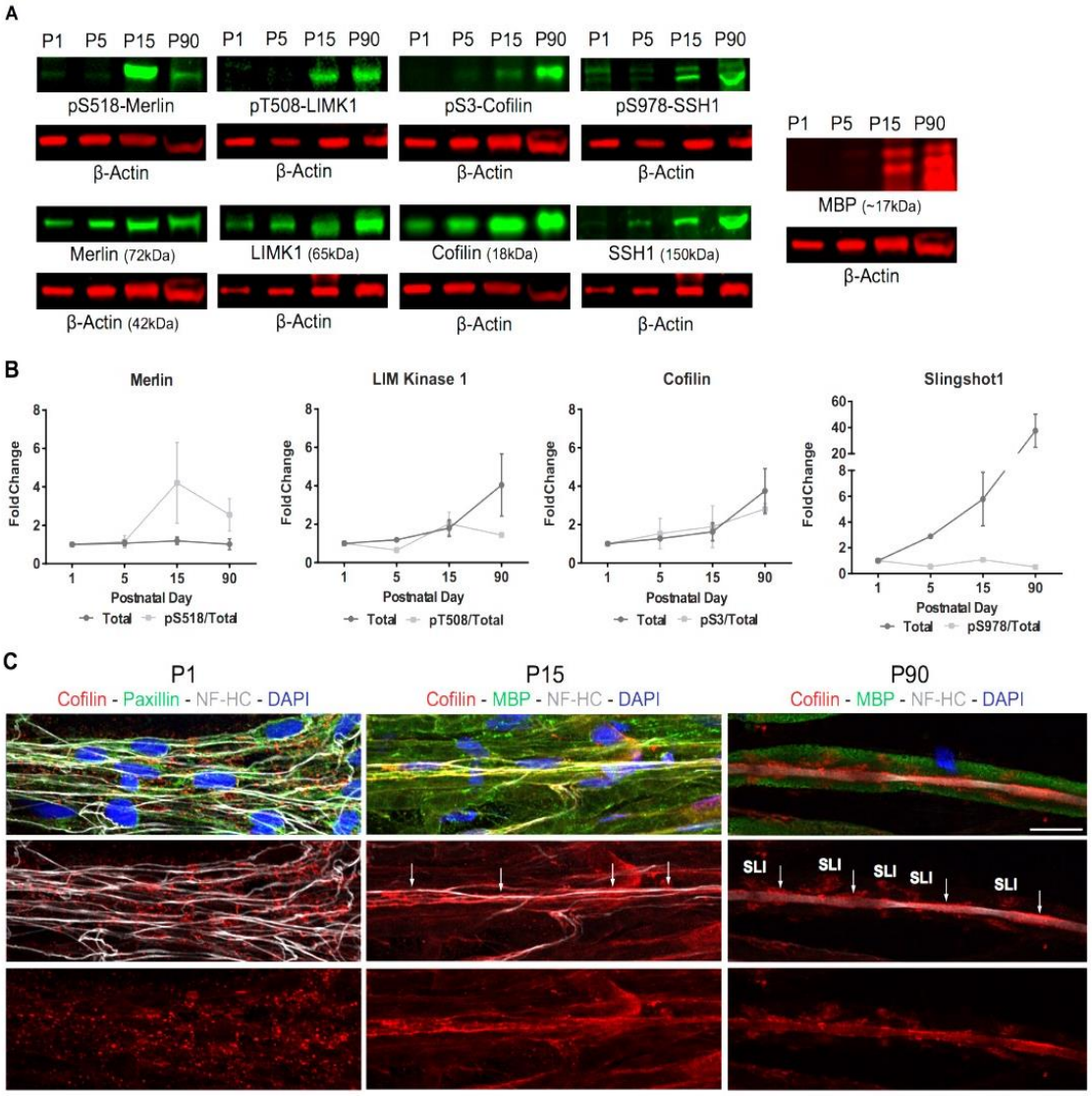

Figure 19. Merlin, LIMK, Cofilin, Slingshot expression and phosphorylation are developmentally regulated in peripheral nerves.

(A) Protein lysates were prepared from sciatic nerves from 1, 5, 15, and 90 day-old rats, and blotted for the indicated total and phosphorylated proteins. (B) Quantitation of immunoblots is shown (n=2 for LIMK1/p-LIMK1 and SSH1/p-SSH1, n=3 for all others). Each signal was normalized to its respective β-actin, phosphorylated protein expressed as a ratio of total protein and expressed as fold change from P1 (signal at P1=1). (C) Teased P1, P15, and P90 rat sciatic nerves were immunostained for cofilin (red), neurofilament-HC (NF-HC; grey), and DAPI. In addition, the P15 and P90 nerves were stained for myelin basic protein (MBP; green) and the P1 nerve was stained for paxillin (green) (adaxonal membrane; arrows). Images are maximum intensity projections.

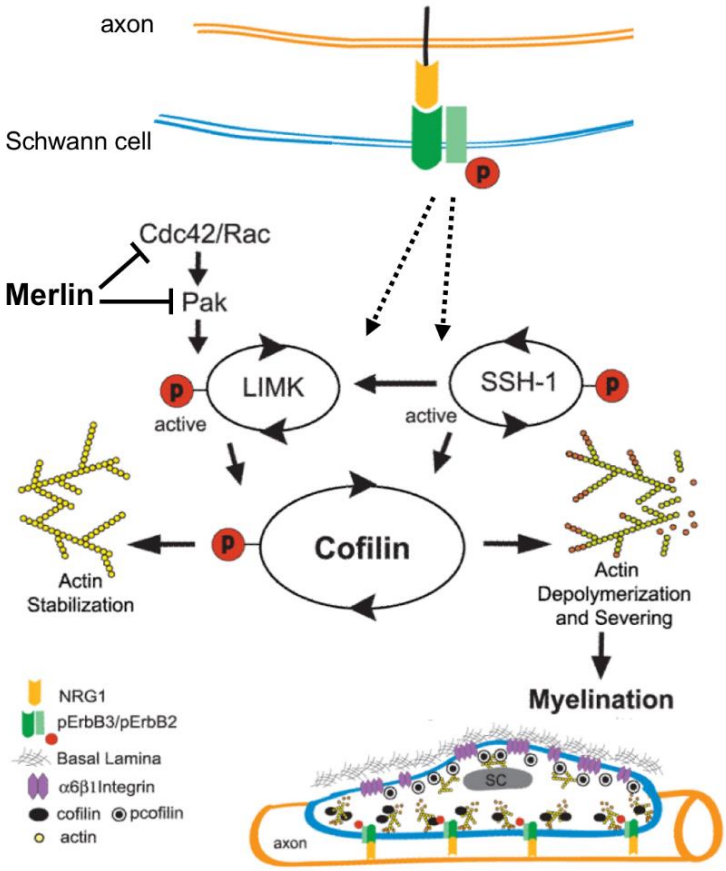

Figure 20. Model of merlin-regulated, neuregulin-dependent activation of cofilin during SC myelination.

Following basal lamina deposition and polarization of the SC, myelination begins as NRG at the adaxonal membrane causes localized activation of cofilin and actin remodeling leading to expansion of the inner mesaxon around the axon. Merlin is needed for activation of cofilin to occur downstream of NRG signaling. In the absence of merlin, Rac-GTP, p-LIMK (active), and F-actin levels are all aberrantly high. We propose that merlin inhibits LIMK indirectly by inhibiting Rac/Pak during NRG induced activation of cofilin. Suppression of these upstream proteins by merlin allows the necessary, and yet to be determined (dashed lines), signaling that leads to simultaneous inhibition of LIMK activity and stimulation of SSH activity downstream of NRG, which ultimately leads to cofilin activation and expansion of the inner mesaxon. In other words, increased LIMK activity in the absence of merlin prevents NRG dependent activation of cofilin. Indeed, pharmacological inhibition of LIMK allows for cofilin activation following NRG stimulation in SCs lacking merlin, and has no effect on cofilin activation in normal SCs.

CHAPTER FOUR: GENERAL CONCLUSION

This thesis has investigated the role of the actin-severing protein cofilin during SC development/maturation, specifically during the process of myelination. This is novel as there have been no other studies that have examined the specific function of an actin depolymerizing protein in SCs. Cofilin is essential to myelination both during the alignment and establishment of the one-to-one relationship between the SC and the axolemma, as well as in the response to NRG induced membrane expansion and wrapping. However, and interestingly, it is not necessary for the motility and proliferation of SCs. This result highlights the importance of studying individual actin regulating proteins at all SC developmental stages to gain insight into how the actin cytoskeleton is regulated during SC myelination, an area that is poorly studied yet vital to understand the basic biology of myelinating SCs.

Moreover, this thesis has shown a novel link between cofilin and the NF2 tumor suppressor merlin broadening the understanding of the molecular basis of NF2. Specifically, merlin is a necessary upstream regulator of cofilin as it permits NRG induced cofilin activation by downregulating the activity of LIM kinase in myelinating SCs through its negative regulation of Rac and p21-activated kinase. This discovery is significant for the NF2 field as it provides further evidence that LIM kinase inhibition could be a viable treatment for individuals suffering with NF2, a disease with no FDA approved drug therapy, as previously suggested by work

published by our laboratory (Petrilli et al., 2014). It should be noted that despite the cytotoxic effect of BMS-5 on rat sensory neurons, a new drug could be synthesized, perhaps based on the molecular structure of BMS-5, that would still inhibit LIM kinase but be harmless to normal tissue.

In addition to the chemical signals from axons and the extra cellular matrix that control differentiation of SCs, developing peripheral nerves experience significant mechanical stimulation during limb growth. This mechanical stimulation causes changes in SC cellular morphology as well as changes in signaling proteins and ultimately gene expression. One pathway involved in this mechnotransduction is the Hippo signaling pathway (Low et al., 2014). In mammals, two kinases named MST and LATS control the activity of two transcriptional co-activators, YAP and TAZ, that when present in the nucleus promote proliferation. LATS, downstream of external stimuli and MST activation, phosphorylates YAP/TAZ which sequesters the co-activators within the cytosol inhibiting proliferation. Signaling through junctional complexes, polarity complexes, and G-protein coupled receptors can all stimulate LATS dependent phosphorylation. Moreover, the actin cytoskeleton can also regulate YAP/TAZ activity through a protein called angiomotin, which inhibits YAP/TAZ. Angiomotin associates with F-actin, allowing YAP/TAZ to enter the nucleus; however, when F-actin is depolymerized, by cofilin for example, angiomotin is free to bind and sequester YAP/TAZ in the cytosol. Recently, a study was published that showed YAP/TAZ were essential to Schwann cell development (Poitelon et al., 2016). The authors conditionally deleted YAP and TAZ in SC and

found that the absence of both of these proteins resulted in server peripheral neuropathy due to a deficiency in axonal sorting. This deficiency was caused by lack of expression of integrins that are not only critical in the transcriptional regulation of developing SCs, but also vital to the normal organization of the ECM and overall structure of mature peripheral nerves.

Furthermore, another recent study investigated the role of YAP downstream of merlin in the repair capacity of SCs following nerve injury (Mindos et al., 2017). After nerve damage, SCs dedifferentiate and undergo rapid demyelination transitioning into a repair cell that is dependent upon the expression of the transcription factor c-Jun (Jessen and Mirsky, 2016). These reprogrammed SCs clear cellular debris, promote axonal regrowth through secretion of neurotropic factors, and finally, once axons have regenerated, remyelinate. Mindos et al. conditionally knocked out merlin in SCs and observed a similar mild dysmyelination phenotype, including hyperplasia and short internodes, as seen in the *in vitro* studies presented in this thesis. However, using nerve crush to model injury, they observed that SCs lacking merlin were unable to repair damaged axons as well as remyelinate. The reason for this impairment was an upregulation of YAP in merlin-null SCs. Poitelon et al. reported YAP and TAZ are downregulated in developing peripheral nerves. This is not surprising given the fact that SCs must exit the cell cycle prior to myelination. Thus, in developing SCs YAP/TAZ could be indirectly regulated by cofilin, downstream of merlin, via its regulation of the actin cytoskeleton, and links the work of this thesis to these studies.

Future *in vivo* studies to investigate the phenotype of mice with conditional cofilin loss in developing SC would be of interest. There are several mouse lines that drive expression of Cre recombinase specifically in SCs. These included desert hedgehog- (Jaegle et al., 2003) and the P0-Cre lines (Giovannini et al., 2000) that have been used to conditionally knock out various genes in SCs, including the *Nf2* gene. A recent publication used a novel Cre line where expression of Cre was under the control of the periostin promoter (Gehlhausen et al., 2015). When this line was crossed with the *Nf2*$^{flox2/flox2}$ line, to produce a conditional knock out of merlin in developing SCs, the resulting progeny exhibit a phenotype that more accurately recapitulated the symptoms experienced by NF2 patients than previous models (Giovannini et al., 1999 and 2000). Specifically, mice produced using this periostin-Cre not only developed schwannomas but also exhibited a measureable loss of hearing and balance. Mice with a conditional knock out of cofilin in SCs could be produced by crossing this Cre driver with a mouse line containing a floxed cofilin gene (Gurniak et al., 2005). Based on the *in vitro* data presented in this thesis, it would be expected that these mice would exhibit hypomyelination and an associated decreased nerve function. It would be of interest to compare the phenotype of these cofilin knockout mice with other reported knockout lines to gain further insight into the role of cofilin in developing SCs.

In conclusion, cofilin is the final target downstream of both NRG and laminin signaling, two pathways that are vital to the development of myelinating SCs, and

merlin regulates this signaling dictating the length of the myelin internode. The data presented in this thesis supports the conclusion that the spatiotemporal balance of phosphorylated and dephosphorylated cofilin S3 regulates SC function during myelination. During axon engagement, an increase in cofilin S3 phosphorylation stabilizes F-actin and decreases process motility, allowing for adhesive SC–axon interactions to develop. During active myelination, merlin inhibits the activation of LIM kinase via inhibition of p21-activated kinase and Rac activation, allowing localized dephosphorylation of cofilin S3 at the inner measaxon in response to NRG. This signaling leads to remodeling of the cytoskeleton and triggers directed expansion of the inner plasma membrane ultimately leading to the production of the multilamellar myelin sheath.

REFERENCES

Alfthan K, Heiska L, Grönholm M, Renkema GH, Carpén O. Cyclic AMP-dependent protein kinase phosphorylates merlin at serine 518 independently of p21-activated kinase and promotes merlin-ezrin heterodimerization. J Biol Chem. 2004 Apr 30;279(18):18559-66. Epub 2004 Feb 23. [PubMed: 14981079]

Bernstein BW, Bamburg JR. ADF/cofilin: a functional node in cell biology. Trends Cell Biol. 2010; 20:187–195. [PubMed: 20133134]

Birchmeier C, Nave KA. Neuregulin-1, a key axonal signal that drives Schwann cell growth and differentiation. Glia. 2008; 56:1491–1497. [PubMed: 18803318]

Bravo-Cordero JJ, Magalhaes MA, Eddy RJ, Hodgson L, Condeelis J. Functions of cofilin in cell locomotion and invasion. Nat Rev Mol Cell Biol. 2013Jul;14(7):405-15. doi: 10.1038/nrm3609. Epub 2013 Jun 19. Review. [PubMed:23778968]

Brockes JP, Fields KL, Raff MC. Studies on cultured rat Schwann cells. I. Establishment of purified populations from cultures of peripheral nerve. Brain Res. 1979; 165:105–118. [PubMed: 371755]

Chen LM, Bailey D, Fernandez-Valle C. Association of beta 1 integrin with focal adhesion kinase and paxillin in differentiating Schwann cells. J Neurosci. 2000; 20:3776–3784. [PubMed: 10804218]

Clark MB, Bunge MB. Cultured Schwann cells assemble normal-appearing basal lamina only when they ensheathe axons. Dev Biol. 1989; 133:393–404. [PubMed: 2659405]

Dan C, Kelly A, Bernard O, Minden A. Cytoskeletal changes regulated by the PAK4 serine/threonine kinase are mediated by LIM kinase 1 and cofilin. J Biol Chem. 2001; 276:32115–32121. [PubMed: 11413130]

Denisenko N, Cifuentes-Diaz C, Irinopoulou T, Carnaud M, Benoit E, Niwa-Kawakita M, Chareyre F, Giovannini M, Girault JA, Goutebroze L. Tumor suppressor schwannomin/merlin is critical for the organization of Schwann cell contacts in peripheral nerves. J Neurosci. 2008 Oct 15;28(42):10472-81. doi: 10.1523/JNEUROSCI.2537-08.2008. [PubMed: 18923024]

Dillon RL, Brown ST, Ling C, Shioda T, Muller WJ. An EGR2/CITED1 transcription factor complex and the 14-3-3sigma tumor suppressor are involved in regulating ErbB2

expression in a transgenic- mouse model of human breast cancer. Mol Cell Biol. 2007; 27:8648–8657. [PubMed: 17938205]

Edwards DC, Sanders LC, Bokoch GM, Gill GN. Activation of LIM-kinase by Pak1 couples Rac/ Cdc42 GTPase signalling to actin cytoskeletal dynamics. Nat Cell Biol. 1999; 1:253–259. [PubMed: 10559936]

Fernandez-Valle C, Gwynn L, Wood PM, Carbonetto S, Bunge MB. Anti-beta 1 integrin antibody inhibits Schwann cell myelination. J Neurobiol. 1994; 25:1207–1226. [PubMed: 7529296]

Fernandez-Valle C, Gorman D, Gomez AM, Bunge MB. Actin plays a role in both changes in cell shape and gene-expression associated with Schwann cell myelination. J Neurosci. 1997; 17:241– 250. [PubMed: 8987752]

Gehlhausen JR, Park SJ, Hickox AE, Shew M, Staser K, Rhodes SD, Menon K, Lajiness JD, Mwanthi M, Yang X, Yuan J, Territo P, Hutchins G, Nalepa G, Yang FC, Conway SJ, Heinz MG, Stemmer-Rachamimov A, Yates CW, Wade Clapp D. A murine model of neurofibromatosis type 2 that accurately phenocopies human schwannoma formation. Hum Mol Genet. 2015 Jan 1;24(1):1-8. doi: 10.1093/hmg/ddu414. Epub 2014 Aug 11. [PubMed: 25113746]

Ghosh M, Song X, Mouneimne G, Sidani M, Lawrence DS, Condeelis JS. Cofilin promotes actin polymerization and defines the direction of cell motility. Science. 2004; 304:743–746. [PubMed: 15118165]

Giovannini M, Robanus-Maandag E, van der Valk M, Niwa-Kawakita M, Abramowski V, Goutebroze L, Woodruff JM, Berns A, Thomas G. Conditional biallelic Nf2 mutation in the mouse promotes manifestations of human neurofibromatosis type 2. Genes Dev. 2000 Jul 1;14(13):1617-30. [PubMed: 10887156]

Goebbels S, Oltrogge JH, Kemper R, Heilmann I, Bormuth I, Wolfer S, Wichert SP, Möbius W, Liu X, Lappe-Siefke C, Rossner MJ, Groszer M, Suter U, Frahm J, Boretius S, Nave KA. Elevated phosphatidylinositol 3,4,5-trisphosphate in glia triggers cell-autonomous membrane wrapping and myelination. J Neurosci. 2010; 30:8953–8964. [PubMed: 20592216]

Gohla A, Bokoch GM. 14–3-3 regulates actin dynamics by stabilizing phosphorylated cofilin. Curr Biol. 2002; 12:1704–1710. [PubMed: 12361576]

Gohla A, Birkenfeld J, Bokoch GM. Chronophin, a novel HAD-type serine protein phosphatase, regulates cofilin-dependent actin dynamics. Nat Cell Biol. 2005; 7:21–29. [PubMed: 15580268]

Gomez-Cambronero J. New concepts in phospholipase D signaling in inflammation and cancer. Scientific World Journal. 2010; 10:1356–1369. [PubMed: 20623096]

Gupton SL, Eisenmann K, Alberts AS, Waterman-Storer CM. mDia2 regulates actin and focal adhesion dynamics and organization in the lamella for efficient epithelial cell migration. J Cell Sci. 2007; 120:3475–3487. [PubMed: 17855386]

Gurniak CB, Perlas E, Witke W. The actin depolymerizing factor n-cofilin is essential for neural tube morphogenesis and neural crest cell migration. Dev Biol. 2005 Feb 1;278(1):231-41. [PubMed: 15649475]

Hall A. Rho GTPases and the control of cell behaviour. Biochem Soc Trans. 2005; 33:891–895. [PubMed: 16246005]

Han L, Stope MB, de Jesús ML, Oude Weernink PA, Urban M, Wieland T, Rosskopf D, Mizuno K, Jakobs KH, Schmidt M. Direct stimulation of receptor-controlled phospholipase D1 by phospho- cofilin. EMBO J. 2007; 26:4189–4202. [PubMed: 17853892]

Hotulainen P, Paunola E, Vartiainen MK, Lappalainen P. Actin-depolymerizing factor and cofilin-1 play overlapping roles in promoting rapid F-actin depolymerization in mammalian nonmuscle cells. Mol Biol Cell. 2005; 16:649–664. [PubMed: 15548599]

Huang TY, DerMardirossian C, Bokoch GM. Cofilin phosphatases and regulation of actin dynamics. Curr Opin Cell Biol. 2006; 18:26–31. [PubMed: 16337782]

Jaegle M, Ghazvini M, Mandemakers W, Piirsoo M, Driegen S, Levavasseur F, Raghoenath S, Grosveld F, Meijer D. The POU proteins Brn-2 and Oct-6 share important functions in Schwann cell development. Genes Dev. 2003 Jun 1;17(11):1380-91. [PubMed: 12782656]

Jessen KR, Mirsky R. The origin and development of glial cells in peripheral nerves. Nat Rev Neurosci. 2005 Sep;6(9):671-82. Review. [PubMed: 16136171]

Jessen KR, Mirsky R. The repair Schwann cell and its function in regenerating nerves. J Physiol. 2016 Jul 1;594(13):3521-31. doi: 10.1113/JP270874. Epub 2016 Mar 21. [PubMed: 26864683]

Katoh K, Kano Y, Noda Y. Rho-associated kinase-dependent contraction of stress fibres and the organization of focal adhesions. J R Soc Interface. 2011; 8:305–311. [PubMed: 20826475]

Kissil JL, Wilker EW, Johnson KC, Eckman MS, Yaffe MB, Jacks T. Merlin, theproduct of the Nf2 tumor suppressor gene, is an inhibitor of the p21-activatedkinase, Pak1. Mol Cell. 2003 Oct;12(4):841-9. [PubMed: 14580336]

Kissil JL, Johnson KC, Eckman MS, Jacks T. Merlin phosphorylation by p21-activated kinase 2 and effects of phosphorylation on merlin localization. J Biol Chem. 2002 Mar 22;277(12):10394-9. Epub 2002 Jan 8. [PubMed: 11782491]

Lallemand D, Saint-Amaux AL, Giovannini M. Tumor-suppression functions of merlin are independent of its role as an organizer of the actin cytoskeleton in Schwann cells. J Cell Sci. 2009 Nov 15;122(Pt 22):4141-9. doi: 10.1242/jcs.045914. [PubMed: 19910496]

Salzer JL. Polarized domains of myelinated axons. Neuron. 2003 Oct 9;40(2):297-318. Review. [PubMed: 14556710]

Low BC, Pan CQ, Shivashankar GV, Bershadsky A, Sudol M, Sheetz M. YAP/TAZ as mechanosensors and mechanotransducers in regulating organ size and tumor growth. FEBS Lett. 2014 Aug 19;588(16):2663-70. doi: 10.1016/j.febslet.2014.04.012. Epub 2014 Apr 18. Review. [PubMed: 24747426]

Marshall TW, Aloor HL, Bear JE. Coronin 2A regulates a subset of focal-adhesion-turnover events through the cofilin pathway. J Cell Sci. 2009; 122:3061–3069. [PubMed: 19654210]

Manetti F. LIM kinases are attractive targets with many macromolecular partners and only a few small molecule regulators. Med Res Rev. 2012 Sep;32(5):968-98. doi: 10.1002/med.20230. Review. [PubMed: 22886629]

Maruthamuthu V, Aratyn-Schaus Y, Gardel ML. Conserved F-actin dynamics and force transmission at cell adhesions. Curr Opin Cell Biol. 2010; 22:583–588. [PubMed: 20728328]

Melendez-Vasquez CV, Einheber S, Salzer JL. Rho kinase regulates Schwann cell myelination and formation of associated axonal domains. J Neurosci. 2004; 24:3953–3963. [PubMed: 15102911]

Michailov GV, Sereda MW, Brinkmann BG, Fischer TM, Haug B, Birchmeier C, Role L, Lai C, Schwab MH, Nave KA. Axonal neuregulin-1 regulates myelin sheath thickness. Science. 2004; 304:700–703. [PubMed: 15044753]

Mindos T, Dun XP, North K, Doddrell RD, Schulz A, Edwards P, Russell J, Gray B, Roberts SL, Shivane A, Mortimer G, Pirie M, Zhang N, Pan D, Morrison H, Parkinson DB. Merlin controls the repair capacity of Schwann cells after injury by regulating Hippo/YAP activity. J Cell Biol. 2017 Feb;216(2):495-510. doi: 10.1083/jcb.201606052. Epub 2017 Jan 30. [PubMed: 28137778]

Morrison H, Sperka T, Manent J, Giovannini M, Ponta H, Herrlich P.Merlin/neurofibromatosis type 2 suppresses growth by inhibiting the activation of Ras and Rac. Cancer Res. 2007 Jan 15;67(2):520-7. [PubMed: 17234759]

Mouneimne G, DesMarais V, Sidani M, Scemes E, Wang W, Song X, Eddy R, Condeelis J. Spatial and temporal control of cofilin activity is required for directional sensing during chemotaxis. Curr Biol. 2006; 16:2193–2205. [PubMed: 17113383]

Nagata-Ohashi K, Ohta Y, Goto K, Chiba S, Mori R, Nishita M, Ohashi K, Kousaka K, Iwamatsu A, Niwa R, Uemura T, Mizuno K. A pathway of neuregulin-induced activation of cofilin-phosphatase Slingshot and cofilin in lamellipodia. J Cell Biol. 2004 May 24;165(4):465-71. [PubMed: 15159416]

Niwa R, Nagata-Ohashi K, Takeichi M, Mizuno K, Uemura T. Control of actin reorganization by Slingshot, a family of phosphatases that dephosphorylate ADF/cofilin. Cell. 2002; 108:233–246. [PubMed: 11832213]

Nodari A, Zambroni D, Quattrini A, Court FA, D'Urso A, Recchia A, Tybulewicz VL, Wrabetz L, Feltri ML. Beta1 integrin activates Rac1 in Schwann cells to generate radial lamellae during axonal sorting and myelination. J Cell Biol. 2007; 177:1063–1075. [PubMed: 17576799]

Ohashi K, Nagata K, Maekawa M, Ishizaki T, Narumiya S, Mizuno K. Rho-associated kinase ROCK activates LIM-kinase 1 by phosphorylation at threonine 508 within the activation loop. J Biol Chem. 2000; 275:3577–3582. [PubMed: 10652353]

Oser M, Condeelis J. The cofilin activity cycle in lamellipodia and invadopodia. J Cell Biochem. 2009; 108:1252–1262. [PubMed: 19862699]

Osherov N, Gazit A, Gilon C, Levitzki A. Selective inhibition of the epidermal growth factor and HER2/neu receptors by tyrphostins. J Biol Chem. 1993; 268:11134–11142. [PubMed: 8098709]

Pelton PD, Sherman LS, Rizvi TA, Marchionni MA, Wood P, Friedman RA, Ratner N.Ruffling membrane, stress fiber, cell spreading and proliferation abnormalities in human Schwannoma cells. Oncogene. 1998 Oct 29;17(17):2195-209. [PubMed: 9811451]

Pereira JA, Lebrun-Julien F, Suter U. Molecular mechanisms regulating myelination in the peripheral nervous system. Trends Neurosci. 2012 Feb;35(2):123-34. doi: 10.1016/j.tins.2011.11.006. Epub 2011 Dec 21. Review. [PubMed: 22192173]

Petrilli AM, Fernández-Valle C. Role of Merlin/NF2 inactivation in tumorbiology. Oncogene. 2016 Feb 4;35(5):537-48. doi: 10.1038/onc.2015.125. Epub 2015 Apr 20. Review. [PubMed: 25893302]

Petrilli A, Copik A, Posadas M, Chang LS, Welling DB, Giovannini M, Fernández-Valle C. LIM domain kinases as potential therapeutic targets for neurofibromatosis type 2. Oncogene. 2014 Jul 3;33(27):3571-82. doi: 10.1038/onc.2013.320. Epub 2013 Aug 12. [PubMed: 23934191]

Poitelon Y, Lopez-Anido C, Catignas K, Berti C, Palmisano M, Williamson C, Ameroso D, Abiko K, Hwang Y, Gregorieff A, Wrana JL, Asmani M, Zhao R, Sim FJ, Wrabetz L, Svaren J, Feltri ML. YAP and TAZ control peripheral myelination and the expression of laminin receptors in Schwann cells. Nat Neurosci. 2016 Jul;19(7):879-87. doi: 10.1038/nn.4316. Epub 2016 Jun 6. [PubMed: 27273766]

Poliak S, Peles E. The local differentiation of myelinated axons at nodes of Ranvier. Nat Rev Neurosci. 2003 Dec;4(12):968-80. Review. [PubMed PMID: 14682359]

Ross-Macdonald P, de Silva H, Guo Q, Xiao H, Hung CY, Penhallow B, Markwalder J, He L, Attar RM, Lin TA, Seitz S, Tilford C, Wardwell-Swanson J, Jackson D. Identification of a nonkinase target mediating cytotoxicity of novel kinase inhibitors. Mol Cancer Ther. 2008; 7:3490–3498. [PubMed: 19001433]

Rudge SA, Wakelam MJ. Inter-regulatory dynamics of phospholipase D and the actin cytoskeleton. Biochim Biophys Acta. 2009; 1791:856–861. [PubMed: 19422932]

Salzer JL. Polarized domains of myelinated axons. Neuron. 2003 Oct 9;40(2):297-318. Review. [PubMed: 14556710]

Sehgal BU, DeBiase PJ, Matzno S, Chew TL, Claiborne JN, Hopkinson SB, Russell A, Marinkovich MP, Jones JC. Integrin beta4 regulates migratory behavior of keratinocytes by determining laminin-332 organization. J Biol Chem. 2006; 281:35487–35498. [PubMed: 16973601]

Sidani M, Wessels D, Mouneimne G, Ghosh M, Goswami S, Sarmiento C, Wang W, Kuhl S, El-Sibai M, Backer JM, Eddy R, Soll D, Condeelis J. Cofilin determines the migration behavior and turning frequency of metastatic cancer cells. J Cell Biol. 2007; 179:777–791. [PubMed: 18025308]

Taveggia C, Zanazzi G, Petrylak A, Yano H, Rosenbluth J, Einheber S, Xu X, Esper RM, Loeb JA, Shrager P, Chao MV, Falls DL, Role L, Salzer JL. Neuregulin-1 type III determines the ensheathment fate of axons. Neuron. 2005; 47:681–694. [PubMed: 16129398]

Thaxton C, Lopera J, Bott M, Baldwin ME, Kalidas P, Fernandez-Valle C. Phosphorylation of the NF2 tumor suppressor in Schwann cells is mediated by Cdc42-Pak and requires paxillin binding. Mol Cell Neurosci. 2007; 34:231–242. [PubMed: 17175165]

Thaxton C, Lopera J, Bott M, Fernandez-Valle C. Neuregulin and laminin stimulate phosphorylation of the NF2 tumor suppressor in Schwann cells by distinct protein kinase A and p21-activated kinase-dependent pathways. Oncogene. 2008; 27:2705–2715. [PubMed: 17998937]

Thaxton C, Bott M, Walker B, Sparrow NA, Lambert S, Fernandez-Valle C. Schwannomin/merlin promotes Schwann cell elongation and influences myelin segment length. Mol Cell Neurosci. 2011; 47:1–9. [PubMed: 21182951]

van Rheenen J, Song X, van Roosmalen W, Cammer M, Chen X, Desmarais V, Yip SC, Backer JM, Eddy RJ, Condeelis JS. EGF-induced PIP2 hydrolysis releases and activates cofilin locally in carcinoma cells. J Cell Biol. 2007; 179:1247–1259. [PubMed: 18086920]

von Philipsborn A, Bastmeyer M. Mechanisms of gradient detection: a comparison of axon pathfinding with eukaryotic cell migration. Int Rev Cytol. 2007; 263:1–62. [PubMed: 17725964]

Yamauchi J, Miyamoto Y, Chan JR, Tanoue A. ErbB2 directly activates the exchange factor Dock7 to promote Schwann cell migration. J Cell Biol. 2008; 181:351–365. [PubMed: 18426980]

Yin HL, Janmey PA. Phosphoinositide regulation of the actin cytoskeleton. Annu Rev Physiol. 2003;65:761-89. Epub 2002 May 1. Review. [PubMed: 12471164]

Yonezawa N, Nishida E, Iida K, Yahara I, Sakai H. Inhibition of the interactions of cofilin, destrin, and deoxyribonuclease I with actin by phosphoinositides. J Biol Chem. 1990; 265:8382–8386. [PubMed: 2160454]

Zhou L, Ercolano E, Ammoun S, Schmid MC, Barczyk MA, Hanemann CO. Merlin-deficient human tumors show loss of contact inhibition and activation of Wnt/β-catenin signaling linked to the PDGFR/Src and Rac/PAK pathways. Neoplasia. 2011 Dec;13(12):1101-12. PubMed: 22247700.